NWP SAF

Satellite Application Facility
for Numerical Weather Prediction

Document NWPSAF-MO-TR-024

Version 1.0

12/01/10

Fourth Analysis of the data displayed on the NWP SAF AMV monitoring website

http://www.metoffice.gov.uk/research/interproj/nwpsaf/satwind_report/

James Cotton and Mary Forsythe

Met Office, UK

Fourth Analysis of the data displayed on the NWP SAF AMV monitoring website

James Cotton and Mary Forsythe
Met Office, UK

This documentation was developed within the context of the EUMETSAT Satellite Application Facility on Numerical Weather Prediction (NWP SAF), under the Cooperation Agreement dated 16 December, 2003, between EUMETSAT and the Met Office, UK, by one or more partners within the NWP SAF. The partners in the NWP SAF are the Met Office, ECMWF, KNMI and Météo France.

Change record			
Version	Date	Author / changed by	Remarks
0.1	12/11/09	J Cotton	First draft
0.2	08/12/09	M Forsythe	Updated by Mary Forsythe
0.3	14/12/09	J Cotton	Updated by James Cotton
0.4	15/12/09	M Forsythe	Minor updates by Mary Forsythe
0.5	07/01/10	J Cotton	Updated following review by Roger Saunders and John Eyre
1.0	12/01/10	J Cotton / M Forsythe	Final version for circulation

Contents Page

Fourth Analysis of the data displayed on the NWP SAF AMV monitoring website

James Cotton and Mary Forsythe

1. Introduction

The main aim of the NWP SAF AMV monitoring analysis reports is to improve our understanding of the AMV errors, which in turn may lead to improvements to the derivation and assimilation, and ultimately impact on NWP forecasts. The aims and background to the NWP SAF AMV analyses are described in the 2nd analysis report (Forsythe & Doutriaux-Boucher, 2005). Subsequent analyses build on results of earlier reports and will refer back to these where relevant.

The format of the report is similar to previous analyses with sections highlighting recent developments, feedback on new data types, features identified in the monitoring and a revised action list.

2. Recent developments

The AMV monitoring on the NWP SAF site has undergone a number of changes in the two years since the 3rd analysis report was produced.

- New buttons (see Figure 1) were added to the monthly monitoring in July 2009 to enable easy switching between corresponding plots from different months and years. This is particularly useful for looking at seasonal patterns in the statistics.

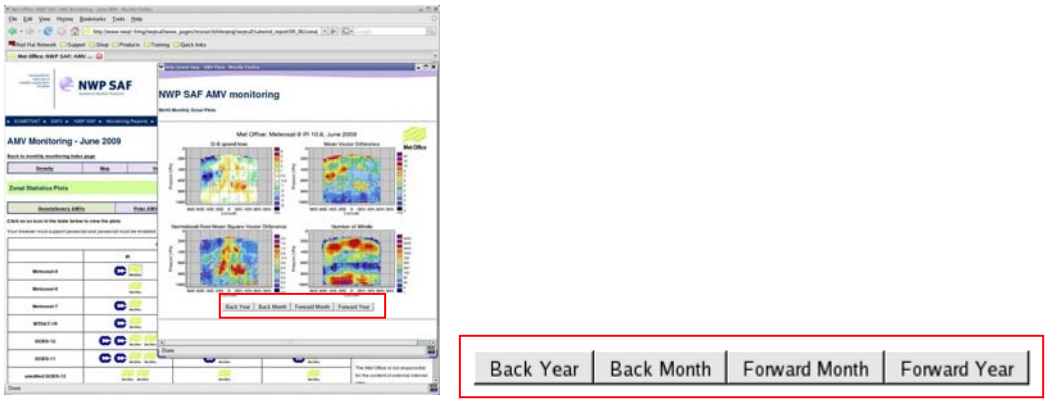

Figure 1: *Example of the NWP SAF AMV monitoring pages, including the new buttons.*

- An investigation section was added to the website in September 2008, which can be viewed at: http://www.metoffice.gov.uk/research/interproj/nwpsaf/satwind_report/investigations.html. This page provides links to one-off or occasional investigations of specific aspects of the AMV monitoring and aims to address items listed in section 5 of the NWP SAF AMV action list. Two investigations have been added which looked at O-B statistics as a function of: (1) height assignment method (added September 2008) and (2) time of day (added July 2009).

- The information on how AMVs are used in different global NWP systems has been updated – see http://www.metoffice.gov.uk/research/interproj/nwpsaf/satwind_report/amvinfo.html.

- The consistency between Met Office and ECMWF speed bias density plots has been improved by aligning the colour scales (January 2008) and standard deviation calculation (September 2008).

- The ECMWF zonal mean vector difference calculation was corrected (January 2008).

- Several new datasets have been added over the last two years including the NOAA-19 AVHRR polar winds, MODIS/AVHRR winds from new direct broadcast stations and the Meteosat-8 rapid scan winds. A summary of the new data types can be found in Section 4 of this report.

For details of planned developments to the NWP SAF AMV monitoring see the action list in the Appendix.

3. Methodology

3.1. NWP SAF AMV monitoring

There are four types of plot available from the NWP SAF AMV monthly monitoring page (see Table 1).

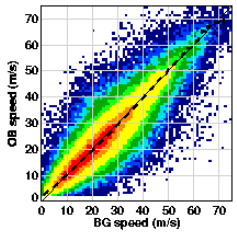	**Speed bias density** Observation wind speed against background wind speed	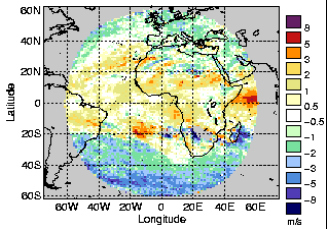	**Map** 1. speed bias 2. mean vector difference 3. normalised root mean square vector difference 4. number
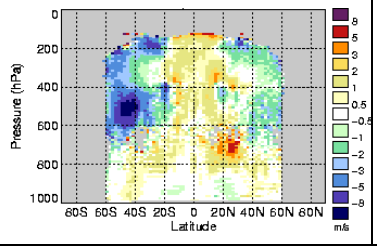	**Zonal** 1. speed bias 2. mean vector difference 3. normalised root mean square vector difference 4. number	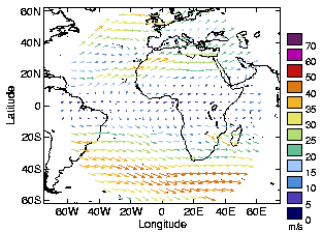	**Vector** 1. mean observed vector 2. mean background vector 3. mean vector difference

***Table* 1:** *Examples of the monthly O-B statistics plots displayed on the NWP SAF AMV monitoring site.*

The monitoring statistics are calculated by comparing wind observations with 6 hour model forecasts valid at the observation times. Both the AMVs and the model forecast contribute to the differences seen in the plots; neither can be assumed to be true. But by comparing plots of the same observations against different NWP backgrounds, it may be possible to separate error contributions from the observations and models. The aim of the NWP SAF AMV monitoring is to provide easily comparable plots from different centres (Met Office and ECMWF) so that similarities and differences can be easily recognised.

All plots in this report, unless stated otherwise, are produced using observations with quality indicator (QI) values greater than 80 for the geostationary winds and greater than 60 for the polar winds (where the QI is the EUMETSAT-designed QI without first guess check). For more information on the EUMETSAT quality indictor see Holmlund (1998). Throughout this document NH refers to the area north of 20N, SH refers to the area south of 20S and the tropics refers to the area between 20S and 20N.

3.2. Model best-fit pressure comparisons

In order to better understand the pattern and cause of features observed in the NWP SAF monitoring, it has been informative to make use of additional statistics. One example is a comparison of the AMV assigned pressure to model best-fit pressure. The model best-fit pressure is calculated by: (1) finding the model level below 100 hPa with the smallest vector difference between the AMV and model background wind and (2) vertically interpolating to find the minimum using a parabolic fit to this model level and the two neighbouring levels. Filters are then applied to the data.

- Remove winds with a minimum vector difference of greater than 4 m/s to avoid cases where there is poor agreement at all levels between the AMV and model wind.

- Remove winds that have a vector difference less than the minimum vector difference + 2 m/s outside of a band +/- 100 hPa from the best-fit pressure. This is designed to eliminate cases where there are secondary minima or very broad minima; in both cases the best-fit pressure is not well constrained (see Figure 2 in the 3rd analysis report).

Care is required when interpreting these results as there are error contributions from the model background wind field and some cases will fail to yield unambiguous best-fit pressures.

3.3. Case studies

Case studies are used increasingly as part of the NWP SAF AMV analysis work to improve our understanding of the relationship between O-B statistics and clouds in the imagery or synoptic flow patterns in the model background field. The potential of the approach was assessed as part of an NWP SAF visiting scientist mission (Galante Negri & Forsythe, 2009); details of the approach are provided below.

1. Use the new buttons described in Section 2 to loop through the monthly NWP SAF AMV monitoring plots to identify months where a feature is particularly prominent.
2. Produce Hovmöller plots for the satellite-channel-month of interest, using additional filtering (e.g. by latitude-longitude) as necessary to narrow down a specific 6-hour run for further investigation
3. Produce map plots for the region of interest showing a range of parameters e.g. AMV pressure, AMV height assignment method, model best-fit pressure, observed and model background vectors etc.
4. Compare map plots with satellite imagery (in some cases overlaying the winds using McIDAS).
5. Where relevant compare AMV heights to other cloud top pressure products including CALIPSO.

4. Assessment of new AMV observation types

4.1 Introduction

This section provides an assessment of new observation types that have been added to the NWP SAF AMV monitoring. The new data types considered in this report are the NOAA-19 polar winds, direct broadcast MODIS and AVHRR winds and Meteosat-8 rapid scan winds.

4.2 NOAA-19 AVHRR polar winds

Polar winds are derived from AVHRR imagery from the NOAA satellite series and MODIS imagery from Aqua and Terra. NOAA-19 was launched on 6 February 2009. The AVHRR winds are produced at NESDIS and CIMSS; the dataset described here is from CIMSS. The main differences to MODIS are: (1) the coarser resolution of 4km (2km used for MODIS) and (2) the lack of a WV channel.

NOAA-19 winds are compared with NOAA 15-18 and MODIS IR winds for August 2009. The NOAA 19 winds show similar timeliness (mean time lag between the time of observation and receipt time) at around 170 minutes to that of NOAA-17 which is the timeliest of the AVHRR winds (Figure 2a). Under normal circumstances we would expect the number of AVHRR winds per month from any of the satellites to be about 50% of the number of MODIS IR winds from Aqua or Terra. This was not the case during the August comparison period due to delays to MODIS data receipt caused by a problem (now resolved) with limited capacity on the Washington GTS link (see Figure 2b).

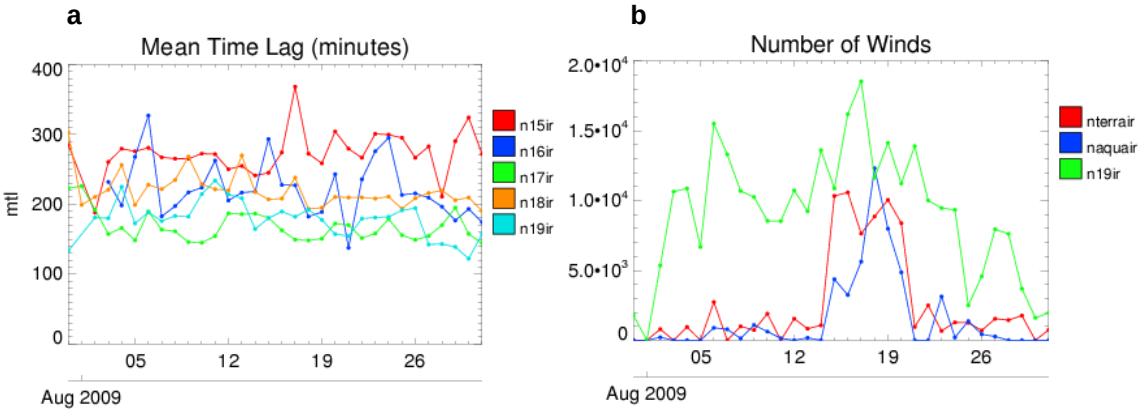

Figure 2: *(a) Mean time lag between observation and receipt time for the AVHRR polar winds and (b) data volume for NOAA-19, Aqua and Terra during August 2009 (all latitudes).*

There is inevitably some redundancy in the coverage provided by NOAA-19 due to its similar 'afternoon' orbit to NOAA-18. Figure 3, however, demonstrates that we would get improved coverage on some occasions.

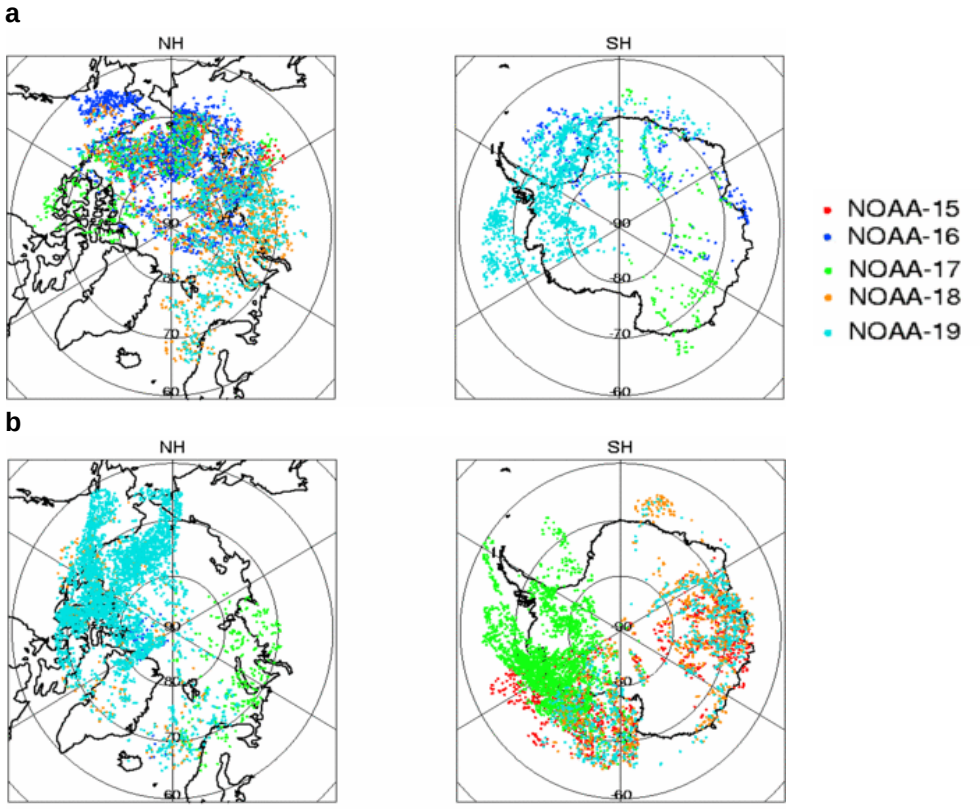

Figure 3: *Data coverage plots showing the distribution of all AVHRR IR winds for (a) 00UTC 7 August 2009, and (b) 12UTC 14 August 2009.*

The AVHRR winds from NOAA-19 show very similar levels of bias and mean vector difference to AMVs from other NOAA satellites (see example in Figure 4).

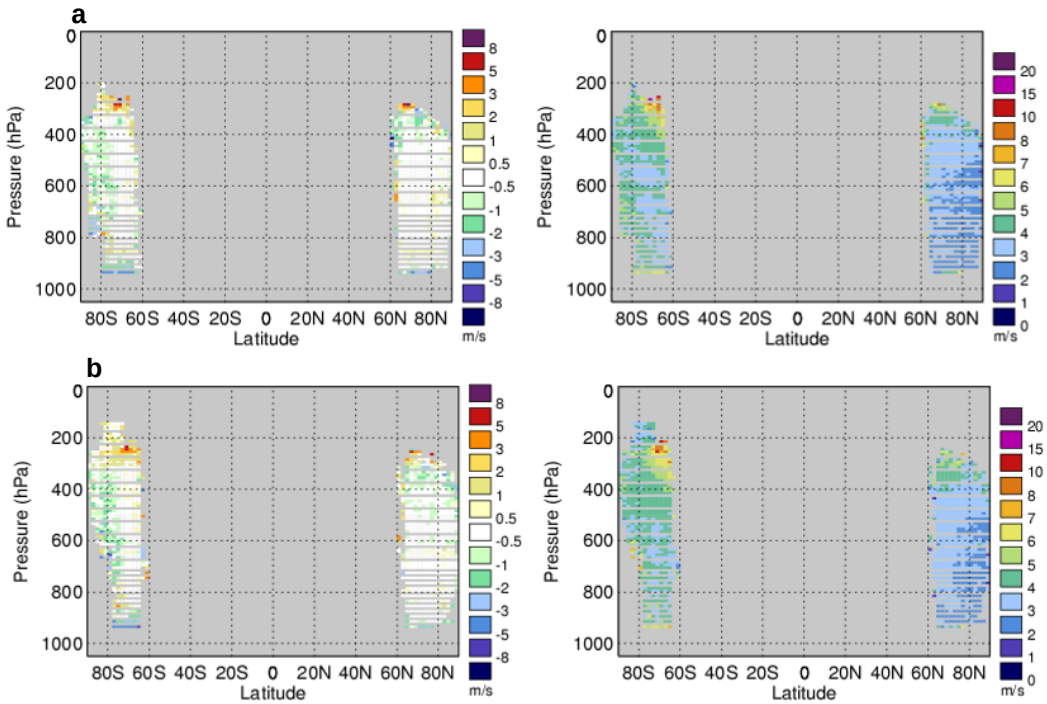

Figure 4: *Zonal O-B speed bias (left) and mean vector difference (right) plots for (a) NOAA-19 and (b) NOAA-15 compared with the Met Office model background for August 2009.*

Collocations of NOAA-19 IR winds with NOAA 15-18 AVHRR winds and MODIS IR winds show NOAA-19 to have similar speeds and directions. The biggest differences are seen in the pressure plots, where NOAA-19 shows a systematic low height bias of between 36-52 hPa in comparison to polar IR winds from all other satellites (independent of height assignment method used). These findings were sent to CIMSS who traced the problem to out-of-date coefficients in the processing code. A fix was applied to the CIMSS winds on 27 October and to the direct broadcast winds on 19 November 2009. Collocations for the period 1 -16 October show much improved pressure statistics e.g. comparing Figures 5 and 6 shows a reduction in height bias from +36 hPa to -2 hPa and a halving of RMS from 48 hPa to 24 hPa.

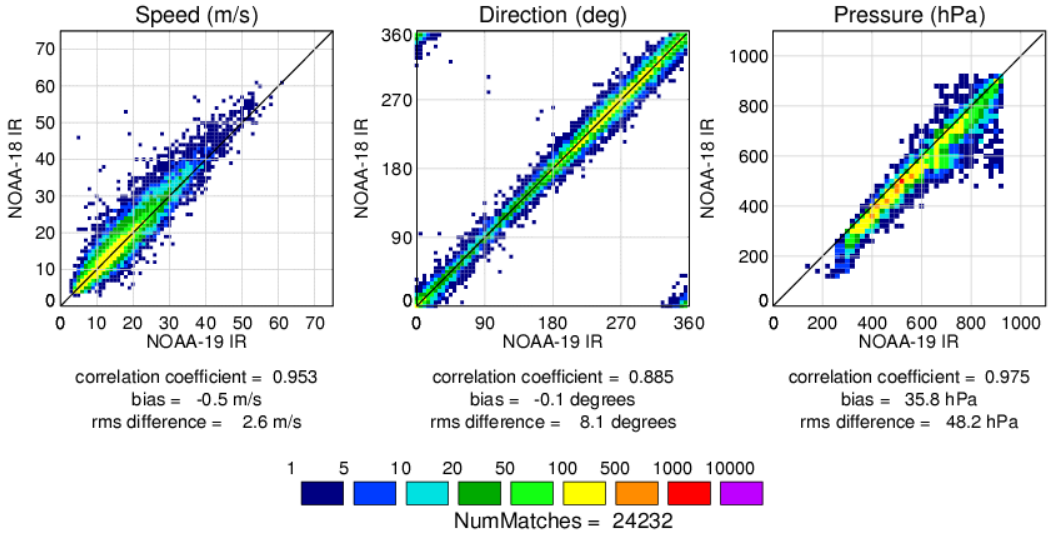

Figure 5: *Collocation plots of speed, direction and pressure differences between NOAA-19 and NOAA-18 for August 2009. The collocation distance and time was 10km and 30 minutes respectively.*

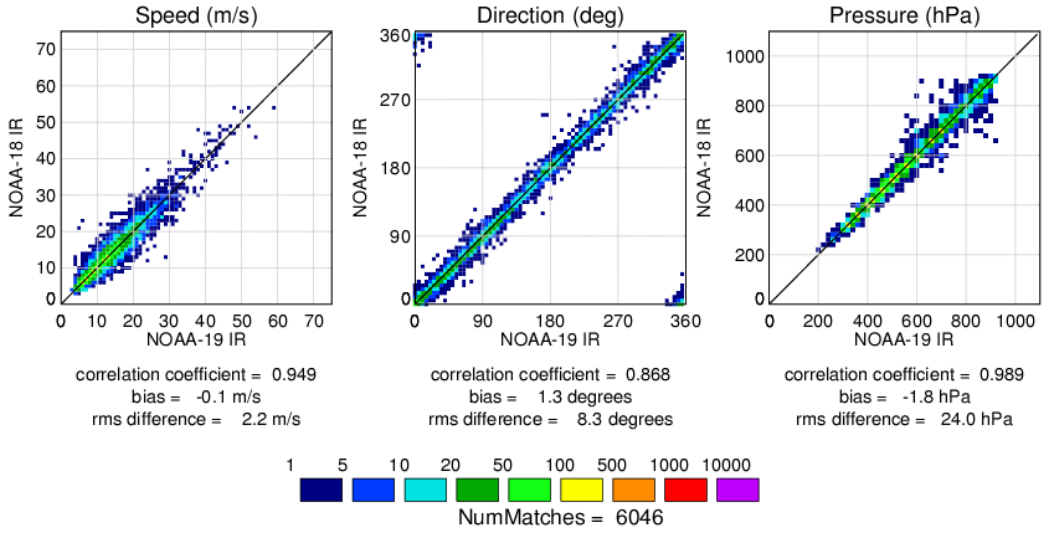

Figure 6: *Collocation plots of speed, direction and pressure differences between NOAA-19 and NOAA-18 for 1 -16 November 2009. The collocation distance and time was 10km and 30 minutes respectively.*

In summary, the statistics for August 2009 show NOAA-19 winds to have similar quality to other polar IR wind datasets; the only significant difference was a bias in height assignment which has since been corrected. The orbital similarity of NOAA-19 and NOAA-18 means we are unlikely to see large increases in data coverage, but assimilating the extra data will make the system more robust to data outages.

4.3 Meteosat-8 rapid scan winds

EUMETSAT have been using Meteosat-8 to provide a rapid scanning service (RSS) over Europe since May 2008. The imagery is 'rapid' in the sense that there is a reduced time interval between successive images of

5 minutes, compared to the standard 15 minutes interval used for Meteosat-9. This is achieved by scanning a reduced area centred on 9.5E, offset from the northern part of the Meteosat-9 region as shown in Figure 7. Initially the channel selection was limited to IR 10.8 and VIS 0.8 due to hardware limitations at EUMETSAT (as was the case for this investigation) but since 30 July 2009 AMVs have been produced from all channels.

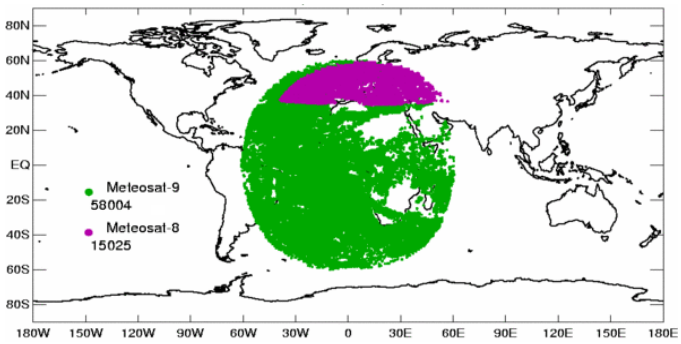

Figure 7: *Plot showing the data coverage of Meteosat-8 whilst in rapid scan mode (purple) over-plotted on the coverage of Meteosat-9 (green) scanning the full Earth disc for 1500-2100 UTC on 4 October 2008.*

Mesoscale wind data is of growing importance to NWP as models, in particular regional models, move to higher spatial resolutions (e.g. Met Office global model moving to 25 km, regional to 12 km, UK to 1.5 km). The Meteosat-8 rapid scan winds are generated using the same target box size (24x24 pixels) and QI formulation as winds produced from 15 minute MSG imagery, although it is recognised that this is unlikely to be optimal for providing information on local-scale flow. Work to develop mesoscale AMV products has been undertaken at a number of centres (e.g. Bedka & Mecikalski, 2005), but it is still early days in learning how best to produce and make use of these products. Some of the main challenges include:

1. Poorer low speed winds (limited by pixel resolution and image interval e.g. 4 km, 5 min - > 13.3 m/s to move one pixel).
2. Existing quality control measures (spatial/temporal consistency, NWP forecast comparisons), may be penalised where the flow is more complex (e.g. tight curvature around a low pressure system). Are there other ways to remove bad data?
3. To constrain the local flow in high resolution NWP we might want to assimilate the mesoscale AMVs at higher spatial and temporal resolution, but they have correlated errors which are largely not accounted for in data assimilation systems.

The Meteosat-8 IR 10.8 and VIS 0.8 winds are compared to Meteosat-9 observations for the same area (latitude: 37N-60N, longitude: 30W-40E). Meteosat-8 rapid scan winds show good timeliness with less than a 30 minute time lag between observation time and receipt time, 10 minutes earlier on average than data from Meteosat-9 (Figure 8a). For the same geographic area, Meteosat-8 provides 2-3 times the number of winds (Figure 8b), mainly due to the production of AMVs every 20 minutes rather than every hour. However, there are some outages. Figure 8b shows the typical 2 day outage of Meteosat-8 once per month, which is required to perform full earth scanning for navigation. There is additionally a one month outage each year to perform full earth scanning and there may be interruptions if backup is required for the 0 degree service.

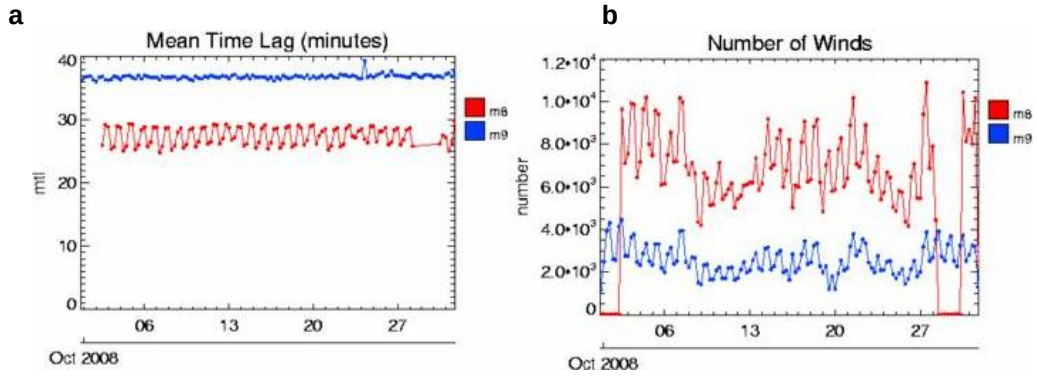

Figure 8 *Data volume and mean time lag between observation and receipt time for Meteosat-8 and Meteosat-9 IR and VIS winds for October 2008. Observations were filtered by latitude (37N-60N) and longitude (30W-40E) for better comparison.*

Comparison of time series plots show that Meteosat-8 rapid scan winds generally have worse RMS vector difference statistics than Meteosat-9 (Figure 9). This remains the case even when slower winds (<10 m/s) are removed (examples not shown). The exception is the mid level IR rapid scan winds which show similar or less bias than Meteosat-9, in an area where we usually see a pronounced slow speed bias.

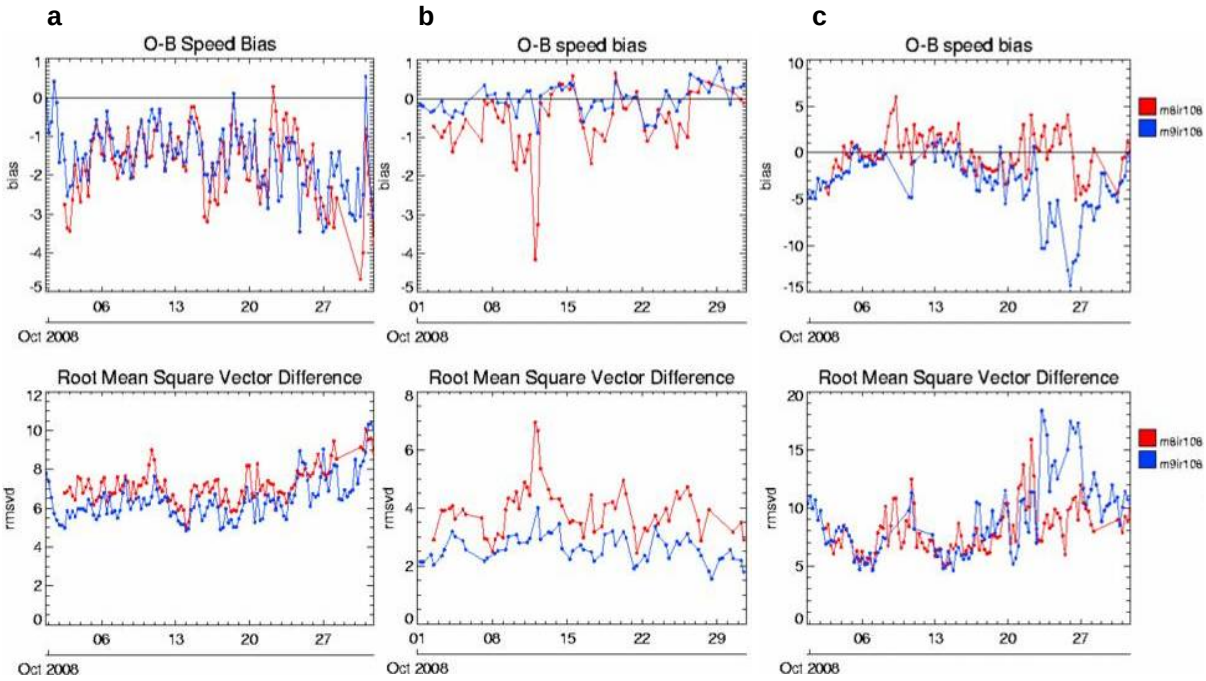

Figure 9: *Time series plots of O-B speed bias and RMS vector difference for Meteosat-8 and Meteosat-9 for October 2008 compared with the Met Office model background: a) IR 10.8 high level, b) VIS 0.8 low level and c) IR 10.8 mid level.*

The NWP SAF map and zonal plots show worse statistics for Meteosat-8 than Meteosat-9 at low and high level, but some improvement at mid level. Figure 10 shows an example of the reduced mid level bias for Meteosat-8 compared with Meteosat-9. The differences may be partly due to the more westerly location of Meteosat-9, which captures more of the jet slow bias, but the statistics are better even in the areas where the coverage overlaps.

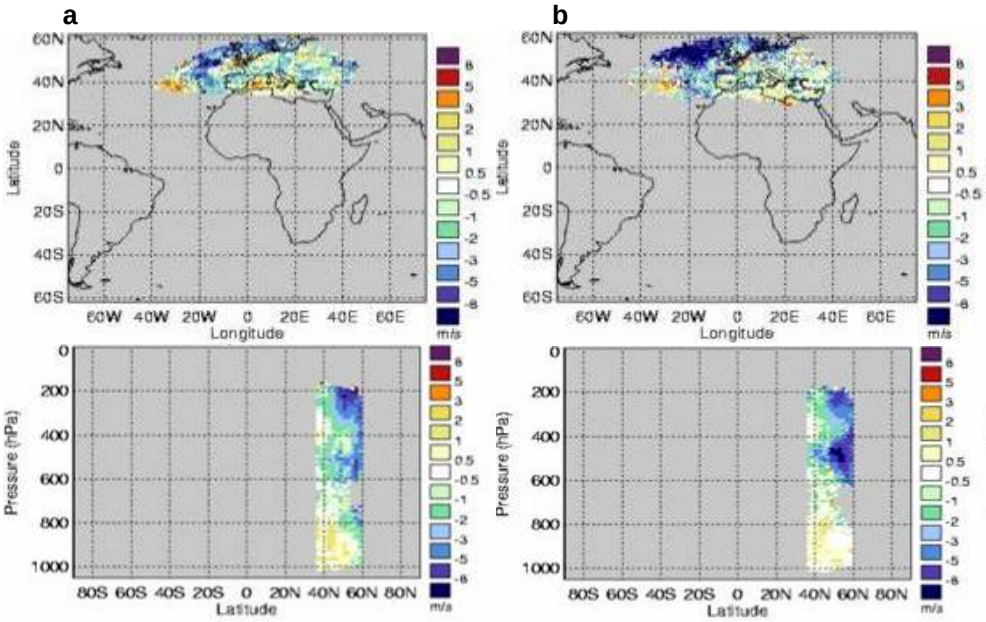

Figure 10: *Map (mid level) and Zonal O-B plots for a) Meteosat-8 and b) Meteosat-9 compared with the Met Office North Atlantic European (NAE) regional model for October 2008.*

Plots comparing speed, direction and height assignment of collocated Meteosat-8 and Meeosat-9 IR and VIS 0.8 AMVs show good consistency in speed and direction, but some marked discrepancies in heights (Figure 11), in particular the area circled in red.

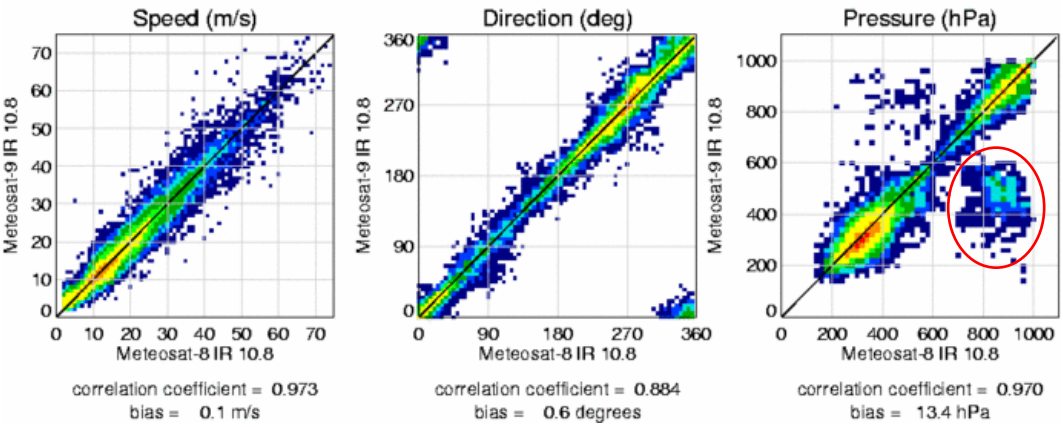

Figure 11: *Plot comparing the speed, direction and pressure of collocated IR10.8 Meteosat-8 rapid scan winds with Meteosat-9 for October 2008. The collocation criteria were observations within 10km and up to 30 minutes apart.*

In order to understand where this difference is coming from the collocations were separated by height assignment method. The area of poor consistency was found to be related to the use of EBBT height assignment for Meteosat-8 and CO_2 slicing for Meteosat-9 (Figure 12a). The opposite scenario occurs, but much less frequently. The use of CO_2 slicing versus EBBT for height assignment is partly determined by a CO_2 cloud top temperature threshold of 253K (EBBT used if warmer). Figure 12b shows that there is a slight bias near 253K in the CO_2 cloud top temperatures for the two satellites which is probably related to a known bias in the CO_2 channel on Meteosat-9 (Hewison and König, 2008). We compared the heights for these mismatched cases to model best-fit pressure to investigate whether Meteosat-8 (EBBT) or Meteosat-9 (CO_2 slicing) show better fit. The results for October 2009 show a roughly equal split.

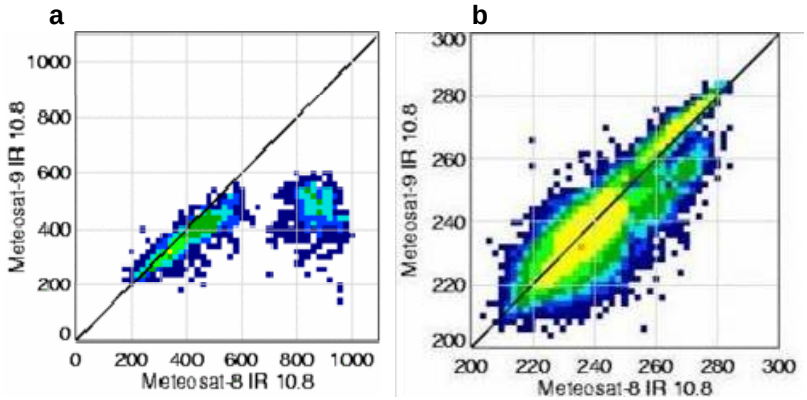

Figure 12: *Plots comparing a) assigned pressures for Meteosat-8 IR 10.8 filtered by the EBBT height assignment method versus Meteosat-9 IR 10.8 filtered by the CO_2 slicing method. b) Plot comparing the CO_2 temperatures of collocated Meteosat-8 and Meteosat-9 winds.*

Standard O-B monitoring is useful as part of an initial evaluation of the Meteosat-8 rapid scan winds, but to learn whether we are getting information at smaller scales, which may benefit higher resolution models, it is more informative to look at case studies. An example is shown for 0300-0900 UTC on 6 February 2009. The broadscale situation is shown by the 0600 UTC Met Office analysis chart in Figure 13a. This shows a complex slow moving frontal depression (979mb) centred to the South of the UK which resulted in heavy, prolonged snow across SW England and the Midlands. The corresponding low level Met Office model wind field for the same time is shown in Figure 13b.

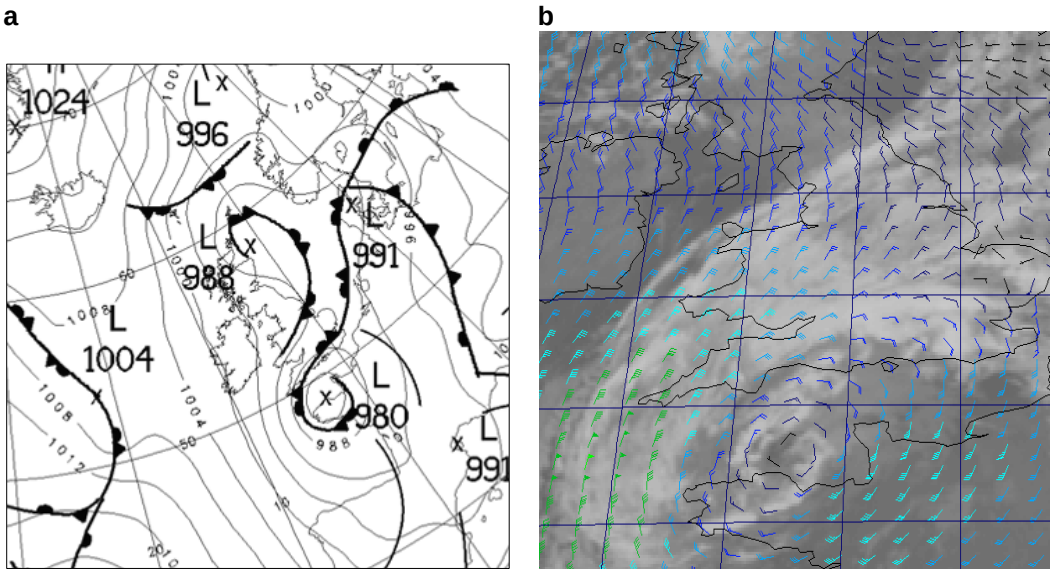

Figure 13: *a) Met Office analysis chart valid 06 UTC on 6 February 2009 cropped to the UK and surrounding area. b) Met Office global model background 850 hPa wind field (UK and NW France), colour-coded by speed, plotted over Meteosat-9 IR 10.8 imagery at 06 UTC using McIdas.*

Visualisation of Meteosat-8 and Meteosat-9 wind vectors valid at 06 UTC on this day (Figure 14) reveals an area of enhanced wind speed across Northern England (yellow vectors) at roughly 400 hPa which is picked up by Meteosat-8, but not by Meteosat-9.

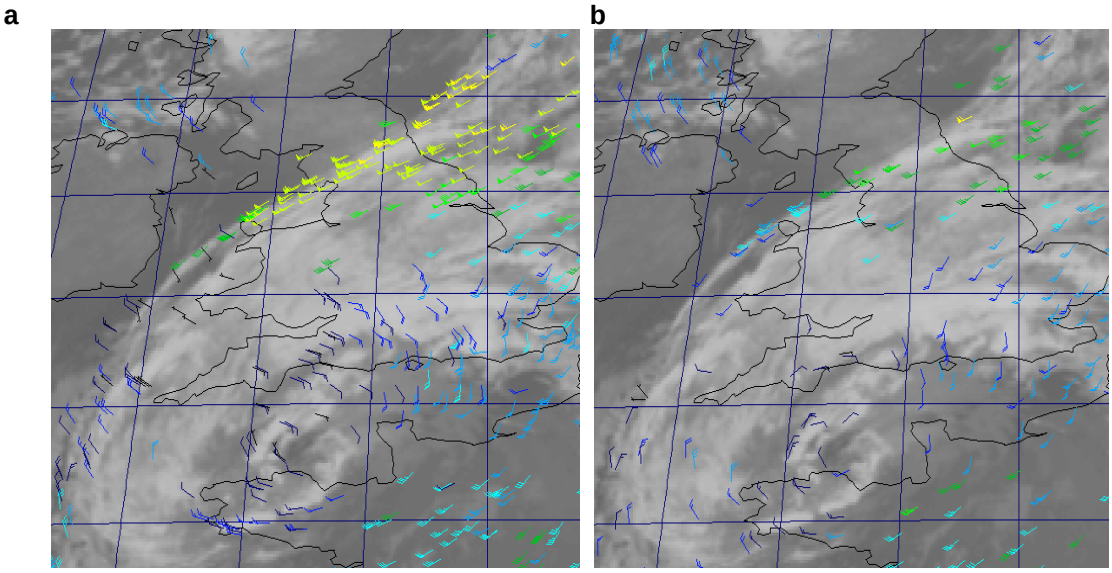

Figure 14: *McIdas visualisation of a) Meteosat-8 rapid scan wind vectors and b) Meteosat-9 wind vectors (all heights) valid at 06 UTC on 6 February 2009, colour-coded by speed and overlain on IR imagery.*

Figure 15 shows more detail near the Channel Islands. Meteosat-8 AMVs show better constraint of the circulation around the centre of the low pressure system. Another noteworthy feature is a discrepancy in height assignment for a group of winds located to the SW of the UK. Meteosat-8 puts the observed 25 m/s winds at about 850 hPa using the EBBT height assignment method in good agreement with the model background. Meteosat-9 puts the observed 20 m/s winds much higher at approximately 550 hPa using the CO_2 slicing method where there is much poorer agreement with the model background (5-10 m/s winds). This is consistent with the difference in height assignment method described in the collocation results.

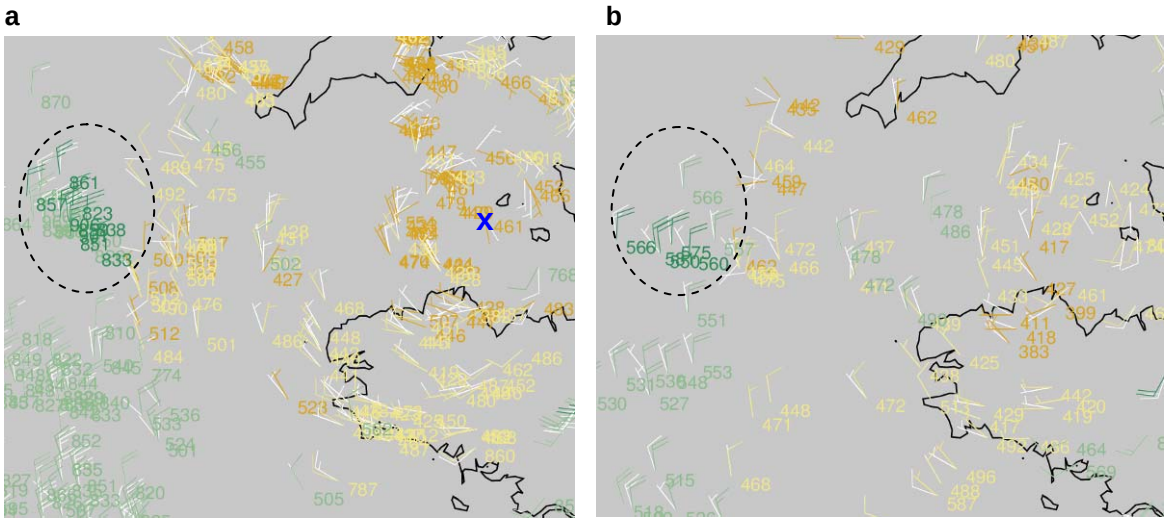

Figure 15: *Visualisation of a) Meteosat-8 rapid scan and b) Meteosat-9 wind vectors valid at 06 UTC on 6 February 2009 colour-coded by speed. Met Office model background wind vectors plotted in white and approximate low pressure centre added by hand in blue.*

In summary, the rapid scan AMVs from Meteosat-8 show poorer statistics than Meteosat-9 at high and low level, but improved results at mid level. The poorer low and high level statistics is only partially explained by problems resolving slower winds. Investigation of several case studies have shown some small improvement in information on local flow from Meteosat-8. More benefit is expected from using smaller target box sizes in the derivation scheme. Further work is planned to assess the more recently provided Meteosat-8 AMVs from the WV and HRVIS channels. The HRVIS channel is of particular interest due to its higher resolution. It is anticipated that work will be required to refine the derivation process for mesoscale winds and to adapt the NWP assimilation and quality control to optimise impact in high resolution NWP.

4.4. New MODIS/AVHRR direct broadcast winds

Background information on development of the direct broadcast polar AMVs is provided in Key et al (2006 and 2008). The direct broadcast winds are produced using the CIMSS AMV derivation system at 6 centres with the main aim to improve timeliness of the data. An analysis of the Tromsø (Norway) and McMurdo Station (Antarctica) direct broadcast data was provided in section 4.3 of the 3rd analysis report. More recently data has become available from Sodankylä in Finland, Fairbanks and Barrow in Alaska and Rothera on the Antarctic Peninsula; a summary is provided here. Figure 16 shows an example data coverage plot.

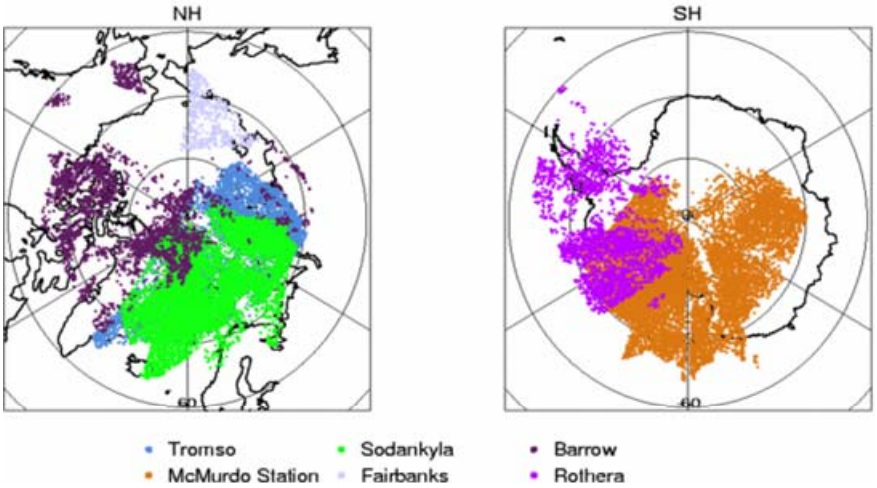

Figure 16: *Data coverage plot showing the location of the direct broadcast MODIS (Tromsø, McMurdo Station, Sodankylä, Fairbanks) and AVHRR (Barrow, Rothera) wind data for the 1200 UTC run on 19 November 2009.*

A summary of the data processed at each station is provided in Table 2.

Direct broadcast station (BUFR originating sub-centre)	Details where multiples centres involved	Satellites processed	Available since:
Tromsø (10)	Downlink: Svalbard Processed: Tromsø	Terra	2006
McMurdo Station (11)		Terra Aqua	2005
Sodankylä (12)		Terra	2007
Fairbanks (13)		Terra (Aqua)	2008
Barrow (14)	Downlink: Barrow Processed: Fairbanks	NOAA-16 NOAA-17 NOAA-18 NOAA-19	2008
Rothera (15)		NOAA-17 NOAA-18 NOAA-19	2009

Table 2: *Summary of the polar direct broadcast AMV data*

The main advantage of the direct broadcast polar AMVs is their improved timeliness of ~100 minutes (see Figure 17) allowing us to assimilate more polar winds in NWP models. The idea is similar to the regional ATOVS retransmission service (RARS) for ATOVS (Griersmith, 2008).

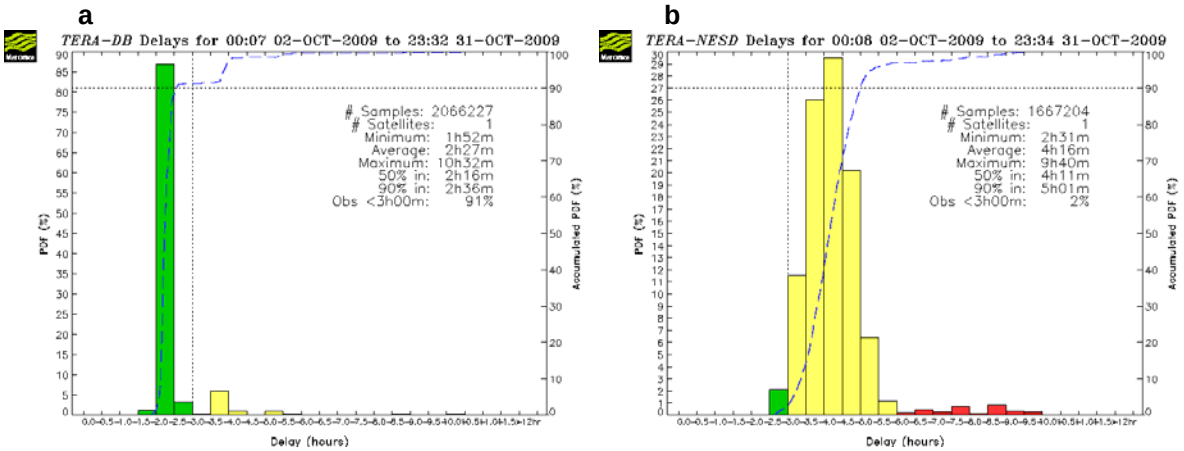

Figure 17: *Histogram plots showing the delay between observation time and receipt time for (a) direct broadcast Terra data and (b) NESDIS Terra data for October 2009.*

Time series plots of RMS vector difference in Figures 18 and 19 indicate the direct broadcast winds are of a similar or slightly better quality compared to the conventional CIMSS or NESDIS polar winds (some differences may relate to differences in coverage). An improvement might be expected for direct broadcast AVHRR winds as the imagery is available at full resolution (derived using 2 km rather than 4 km GAC). The differences for MODIS may relate to differences between the NESDIS and CIMSS derivation schemes.

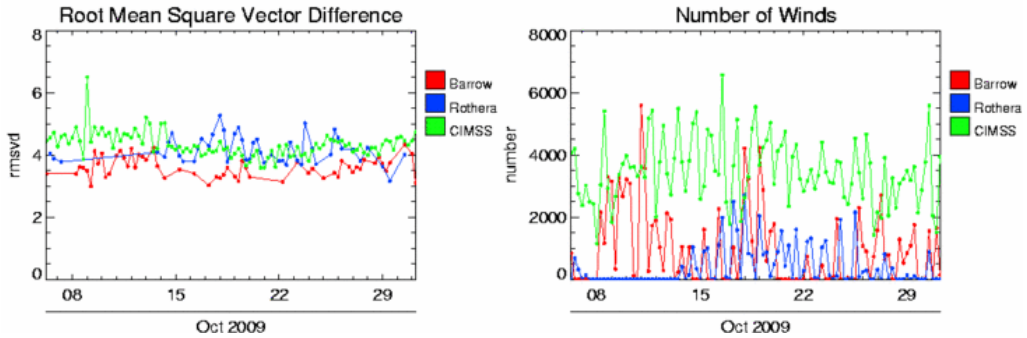

Figure 18: *Time series plots showing the root mean square vector difference and number of winds for AVHRR winds from different sites.*

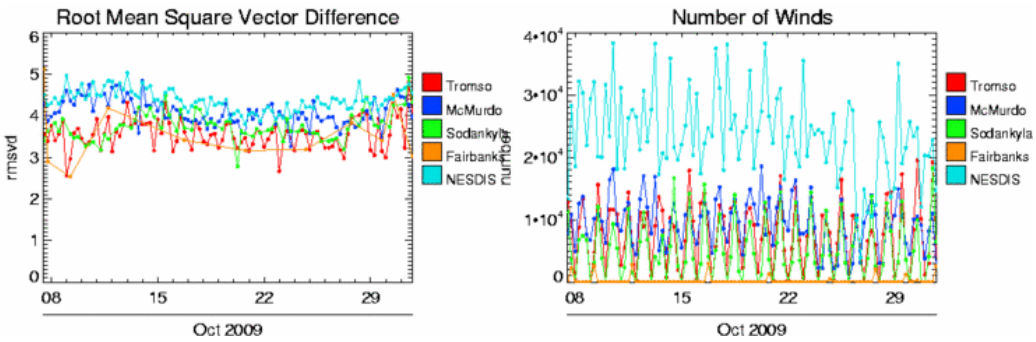

Figure 19: *Time series plots showing the root mean square vector difference and number of winds for MODIS winds from different sites.*

Comparisons of collocated conventional and direct broadcast polar AMVs in Figure 20 show good agreement, particularly for the AVHRR winds which use the same derivation scheme in both cases. A few differences are seen for the MODIS height assignment, which occur when different height assignment methods are used (probably due to slight differences between the NESDIS and CIMSS approaches).

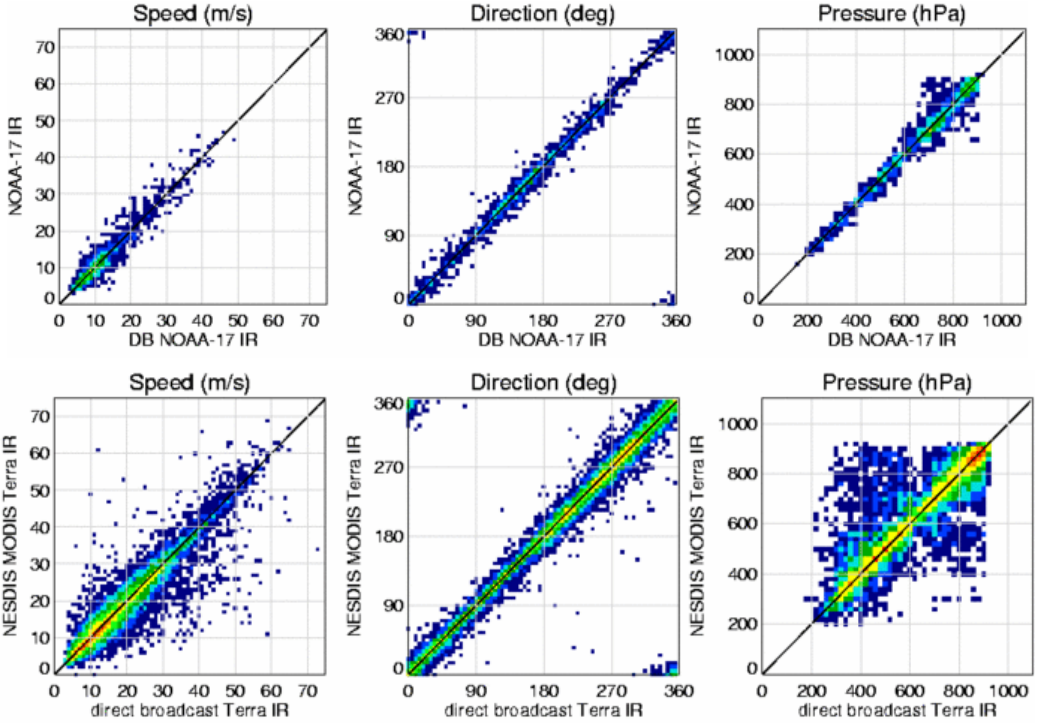

Figure 20: *Plots comparing speed, direction and pressure of collocated (top) CIMSS and Barrow NOAA-17 AMVs and (bottom) NESDIS and Sodankylä Terra IR AMVs. The collocation distance and time were 10 km and 30 minutes respectively.*

In summary, AMV data from the new direct broadcast stations is of comparable or better quality than the conventional polar AMVs and should lead to improved polar AMV coverage, particularly in the shorter cut-off NWP forecast runs, where much of the conventional data arrives too late.

5. Features observed in the O-B statistics plots

5.1. Introduction

The format of Section 5 follows the structure of previous reports where features are discussed in turn. The features are referenced x.y, where x is the number of the analysis report where the feature was first described (i.e. 4 for new examples and 2 or 3 for features noted in the second or third analyses) and y is the

example number. For ease of reading, the geostationary AMV features are subdivided into low level (below 700 hPa), medium level (400-700 hPa) and high level (above 400 hPa), with a separate section for polar AMVs.

Some of the features have been fairly comprehensively described in previous analysis reports. An update is only included in this report for features where further investigation has yielded new results. Two tools that have been used to a greater extent in this analysis compared to previous analyses are examination of (1) seasonal variation using the new buttons described in Section 2 and (2) case studies. The aim is to identify, where possible, the cause of O-B features and any relevant actions that may help to alleviate the problems.

Table 3 summarises the status of each feature and indicates whether further information is provided in this report. A few features described in the second and third analyses are no longer evident in the monthly O-B plots. In some cases this is due to known improvements in AMV derivation or bug fixes (e.g. Feature 3.1). These features are classed as closed and will not be reviewed in future analyses. In some cases the names of features may have been updated to better reflect the pattern or cause.

Ref.	Feature	Resolved?	Update?
LOW LEVEL			
2.1.	GOES fast bias in inversion regions	No	No
2.3.	NE America winter slow speed bias	No	No
2.4.	Fast bias at 40S-60S for Meteosat satellites	No significant signal - close	No
2.6.	Fast bias over Africa	No	Yes
2.7.	Spuriously fast Meteosat and MTSAT-1R winds at low level	No	Yes
4.1.	Slow bias in the equatorial Pacific (Met Office plots only)	No	Yes
MID LEVEL			
2.8.	Fast bias in the tropics	No	Yes
2.9.	Slow bias in the extratropics	No	Yes
3.1.	MTSAT-1R IR fast bias	Yes, 19 May 2009	Yes
HIGH LEVEL			
2.10.	Jet region slow bias	No	Yes
2.11	NESDIS over-correction of slow bias in jets	No	No
2.12.	Indian Ocean fast bias at high level	Less prominent - close	No
2.13.	Tropics fast bias	No	Yes
2.14.	Very high level (above 180 hPa) Meteosat and unedited GOES fast bias	No	No
2.15.	Differences between channels	No	No
3.2.	Very high level (above 180 hPa) Meteosat tropical slow bias	No	No
3.3.	GOES-11 bias change at 180 longitude	No	No
4.2.	GOES near equatorial slow bias	No	Yes
POLAR AMVs			
2.19.	High level fast speed bias	No	Yes
2.20.	Low level slow speed bias in polar IR data	No	Yes
3.4.	NESDIS MODIS IR slow streak	Yes, 27 October 2009	Yes
3.6.	NESDIS-CIMSS polar AMV differences	Improved	No
4.3.	Near-pole mid level slow bias	No	Yes

Table 3: *A summary of the status of features identified in the NWP SAF AMV monitoring.*

In previous reports we have observed that the O-B statistics from the Met Office and ECMWF are very alike. This is still the case. The differences that exist (e.g. Feature 4.1) are mostly in the tropics, which might be explained by the larger model biases in this region. Examples provided in this report are mainly from the Met Office comparisons, but the ECMWF plots show similar results.

5.2. Low Level (below 700 hPa)

The main features of the low level wind field include: (1) faster winds below the jets in the extra-tropics (stronger in winter hemisphere), (2) faster winds associated with tropical cyclones, (3) tropical trade wind easterlies and (4) the seasonal Somali Low-level Jet (see Figure 9 in the 2nd analysis report for example wind field plots). With a few exceptions, the low level AMVs have fairly low O-B mean speed differences, which partly reflects the lower wind speeds in this area.

Update on Feature 2.6. Fast bias over Africa

Fast biases are observed in the IR and visible channels over the Sahara desert, Arabia and Mediterranean. Although present all year, the bias distribution shows seasonal variability. The fast bias is most prominent during the winter months (November-April), when it is located at around 10-30N (e.g. Figure 21), which corresponds fairly well with the location of the high level sub-tropical jet (see Figure 22).

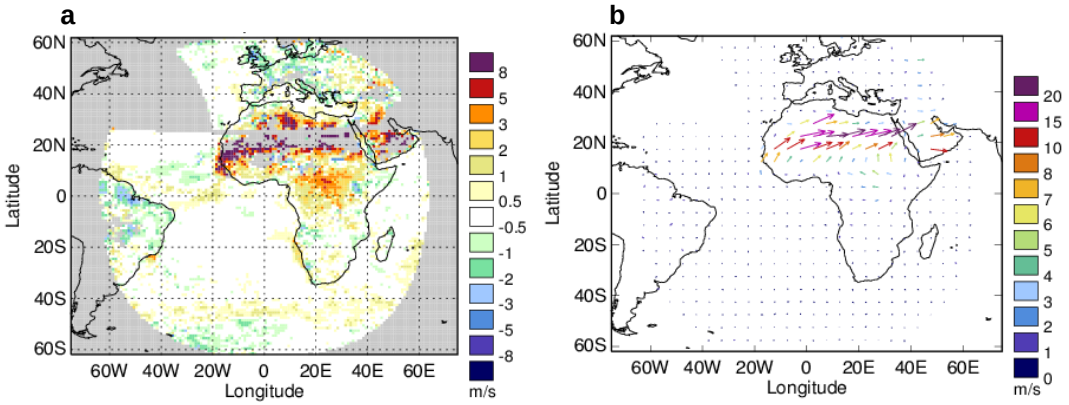

Figure 21: *(a) Map plot of O-B speed bias and (b) mean vector difference for Meteosat-9 HRVIS compared with the Met Office model background for February 2009.*

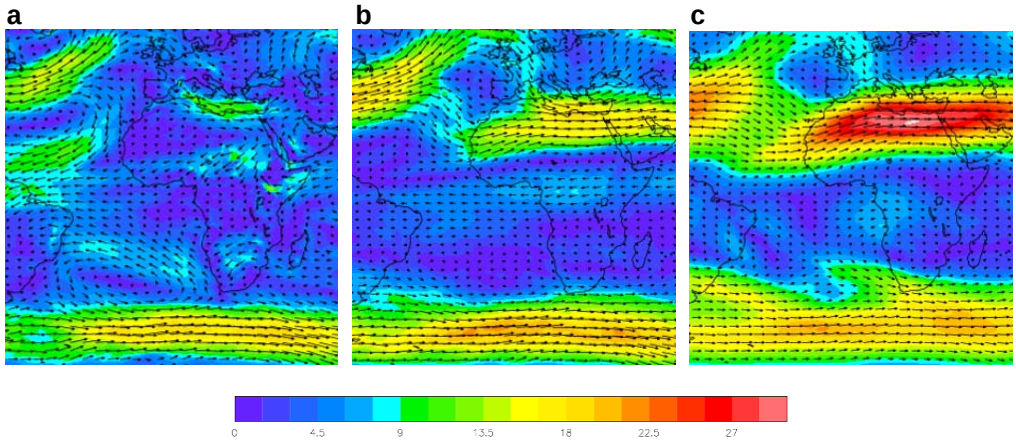

Figure 22: *Mean Met Office analysis wind speed (colour) and vector (arrows) at (a) 850hPa, (b) 500hPa and (c) 200hPa for February 2009.*

In these high wind shear regions a small height assignment error can lead to a significant speed bias. The model best-fit pressure plot (Figure 23) shows low level winds in this area have an average low height bias of around 100 hPa.

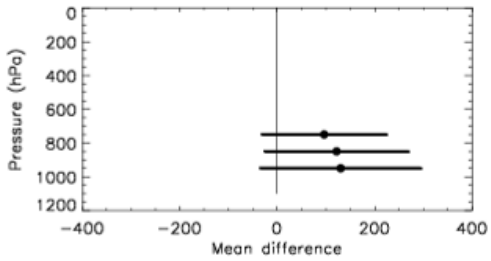

Figure 23: *Mean difference (dots) and standard deviation (bars) of the observed pressure and model best-fit pressure for Meteosat-9 HRVIS AMVs for February 2009. The data has been filtered for those observations over land, 10N-35N.*

A case on 17 February 2009 was chosen for further investigation. On this day the fast bias is associated with a band of observations over land which stretch from North East Libya to Algeria (Figure 24a). The problem AMVs are generally much faster (speeds of up to 40m/s) compared with the surrounding low level observations in the Mediterranean (Figure 24b). The observed and best-fit pressure maps reveal, in the worst case, AMVs with assigned pressures below 900 hPa with model best-fit pressures at around 500 hPa.

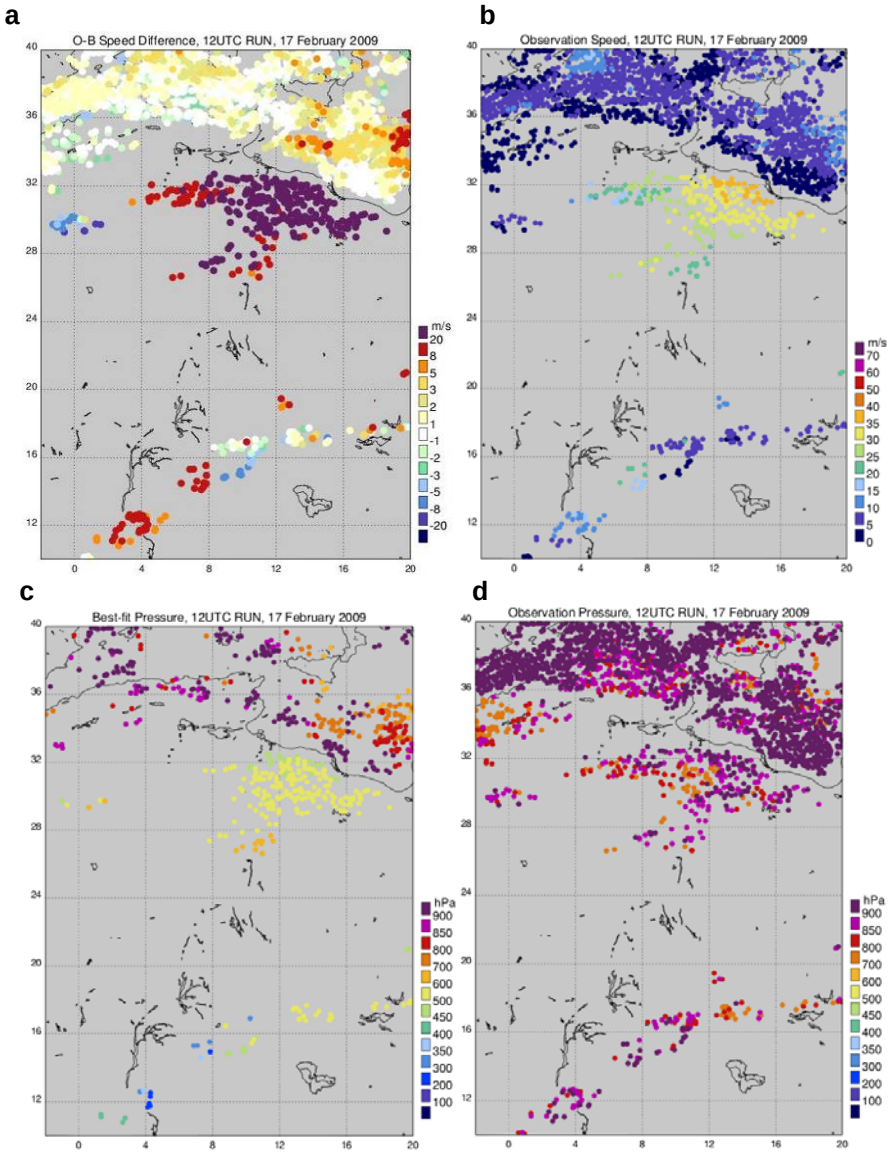

Figure 24: *Map plots showing (a) O-B speed bias, (b) observation speed, (c) model best-fit pressure and (d) assigned pressure for Meteosat-9 HRVIS AMVs valid at 1200 UTC on 17 February 2009.*

The Met Office MSG cloud top height product and visible satellite imagery (Figure 25) are more consistent with a band of high semi transparent cloud. The cloud top height of approximately 20000ft (or 465 hPa) agrees well with the model best-fit pressure. So why are the AMVs being put too low? The AMVs have been assigned cloud base heights, which will tend to put semi-transparent cloud too low due to contributions from below the cloud. The CO_2 slicing pressures at 500-700 hPa show closer agreement, but were not used as the cloud top temperatures were warmer than the 253 K threshold (typically 260-270 K). The IR10.8 AMVs for this case are generally assigned a little higher at 400-700 hPa, but there are still some low level winds with large fast bias.

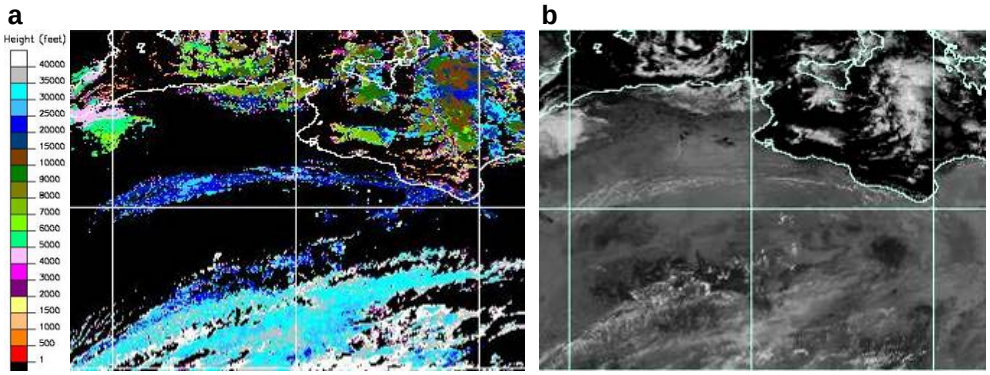

Figure 25: *(a) Met Office MSG product showing the height of the cloud tops in feet for North Africa at 1200 UTC on 17 February 2009. The band of cloud corresponding to the fast bias is shown in dark blue at 20000ft ~ 465 hPa across the centre of the image. (b) Meteosat-9 visible image at 1200 UTC on 17 February 2009.*

During the summer months, the fast bias is normally less prominent and extends further north into the Mediterranean, probably reflecting the weakening and northward shift in location of the high level jet (see Figure 26). A second fast bias is observed close to 15 N during June-July. This corresponds in location to the region of faster mid level easterly winds that cross this region at this time of year (see Figure 26c). As with the winter example shown earlier, the bias probably results from a low height assignment bias in a region of increased vertical wind shear.

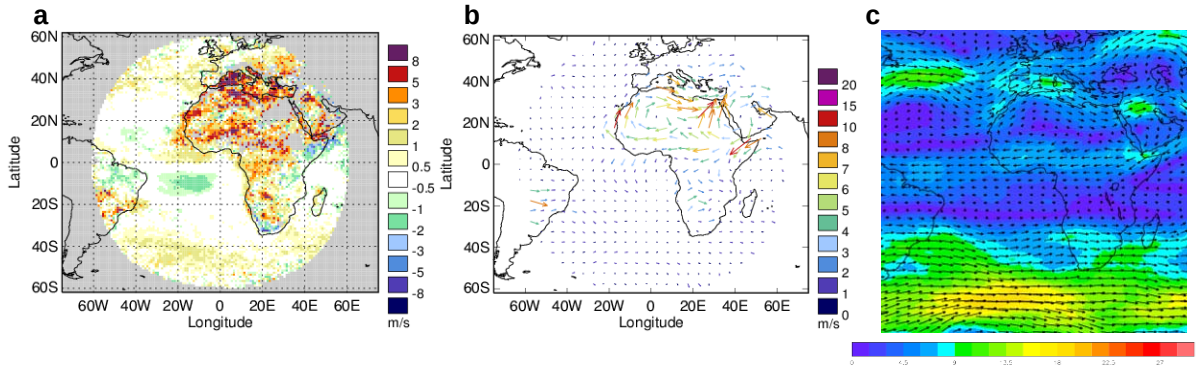

Figure 26: *Maps of (a) O-B speed bias and (b) mean vector difference for low level Meteosat-9 IR10.8 winds for June 2009. (c) Mean Met Office analysis wind speed (colour) and vector (arrows) 500hPa for June 2009.*

Update on Feature 2.7. Spuriously fast Meteosat-7 and MTSAT-1R winds at low level

Meteosat and JMA winds show a number of spuriously fast winds at low level, particularly in regions with high vertical wind shear. In the case of Meteosat-7 we can divide the fast bias into two separate features: (1) the northern Indian Ocean during the monsoon season and (2) below the sub-tropical jet near India during the NH winter.

The fast bias in the northern Indian Ocean is observed from June to October in the IR channel; an example for July 2008 is shown in Figure 27. This feature is less prevalent in the visible channel where the fast bias is confined to a smaller area near the Gulf of Aden. The period June to October coincides with the south-western summer monsoon season in which moisture-laden winds from the Indian Ocean blow into the Indian subcontinent from a south-westerly direction. The low level flow is illustrated by the model background vector

plot in Figure 27b. By contrast, the observed winds in Figure 27a show a much less consistent wind field. There is also an area of less pronounced fast bias at ~15S in the Indian Ocean which develops during the second half of July 2008 (see Figure 28).

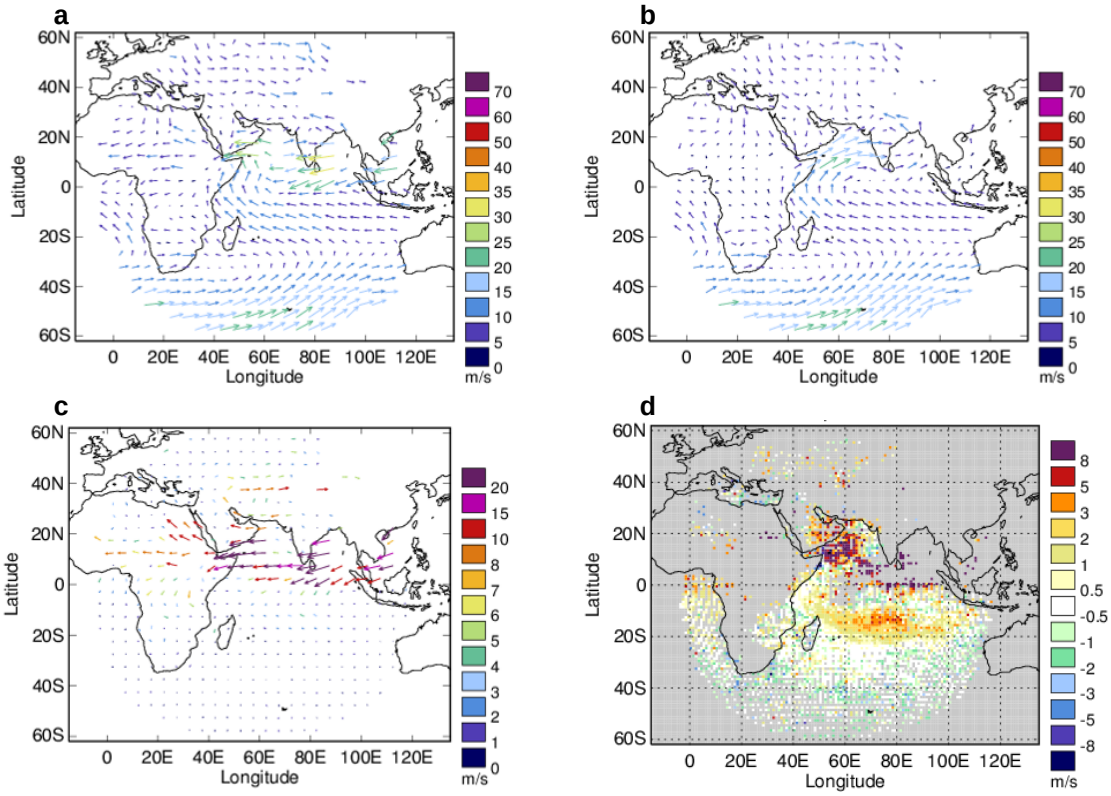

Figure 27: *Vector plots showing (a) the mean observation, (b) the mean background and (c) the mean vector difference for Meteosat-7 IR low level winds for July 2008 compared with the Met Office model background. Plot (d) shows the O-B speed bias plot of Meteosat-7 IR low level winds for July 2008 compared with the Met Office model background.*

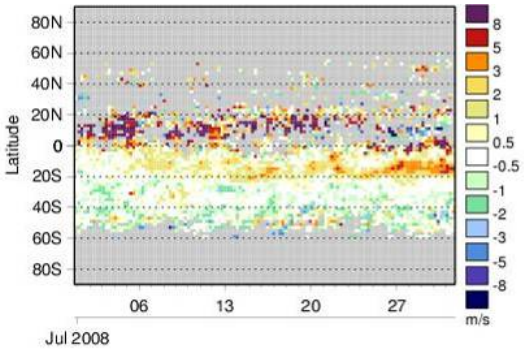

Figure 28: *Hovmöller latitude plot showing the O-B speed bias for Meteosat-7 IR winds compared with the Met Office background for July 2008. The fast bias at 15S seems to develop as the month progresses.*

In the 3rd analysis report it was hypothesised that the unusual patterns seen in the AMV low level wind field are due to faster higher level winds being wrongly assigned to low level. To examine this further a case on 5 July 2008 was chosen for investigation. The vector plot in Figure 29a shows a large number of AMVs to the south and west of India that disagree in speed and direction with the background. The model background vectors are generally less than 20 m/s from the west or south-west, whilst the observed winds are in excess of 40 m/s from the east. CALIPSO data for shortly before 2100 UTC (Figure 29b) shows a mixture of high level clouds at 10-15 km (~100-300 hPa) and broken low level cloud below 4 km (~640 hPa) which is complicated by the presence of aerosol. This is consistent with the hypothesis in the 3rd analysis report that the AMVs may be due to tracking of high level cloud (fast easterly flow in the Tropical Easterly Jet), whilst the height assignment is based on the low level cloud. In these cases, new schemes to better link the pixels

used for tracking and height assignment (e.g. Borde and Oyama, 2008) might help, although there are currently no plans to implement this on Meteosat First Generation.

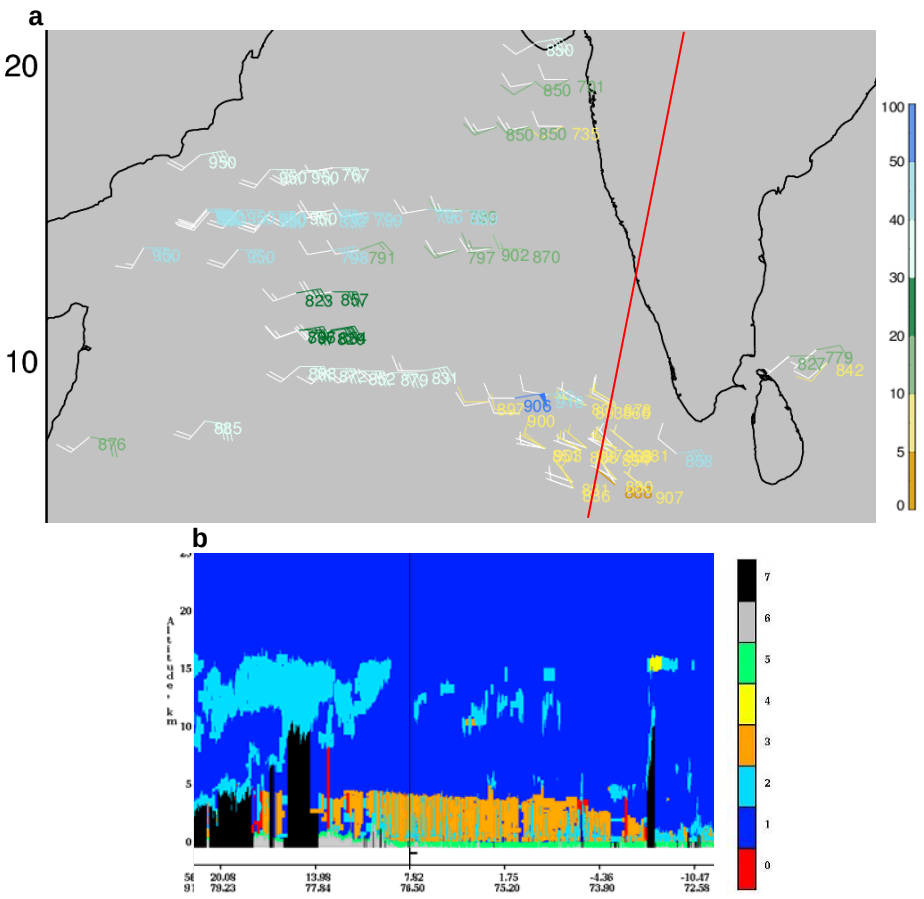

Figure 29: *(a) Vector visualisation plot for Meteosat-7 IR observed and Met Office background winds valid for the 1800 UTC run on 5 July 2008. Vectors are coloured by wind speed in m/s. The red line marks the rough location of a nearby CALIPSO overpass. (b) CALIPSO feature mask for 2043 UTC on the 5 July 2008.*

The Meteosat-7 fast bias is also observed during the winter months when the bias is instead associated with the sub-tropical Jet near India (e.g. Figure 30). The fast bias is most prominent near the Indian subcontinent, in the Bay of Bengal and the Arabian Sea. The AMVs outside of these regions show near neutral bias. The fast bias is not constant throughout February (see Figure 30b).

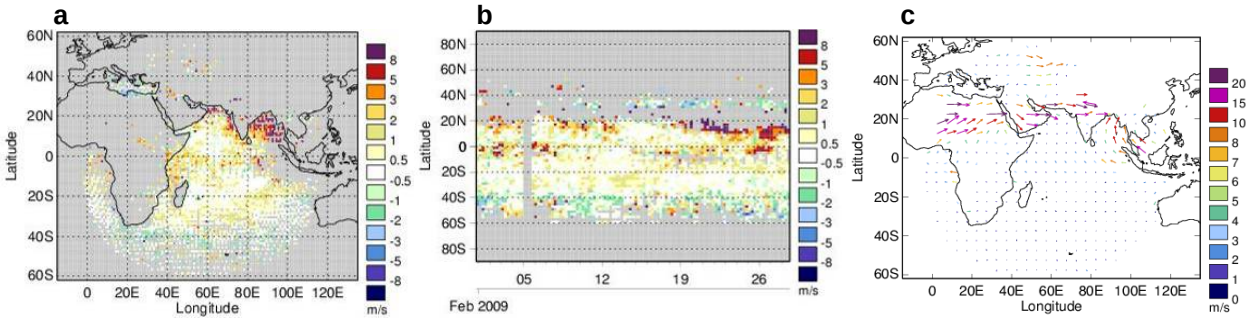

Figure 30: *(a) O-B speed bias plot, (b) Hovmöller O-B speed bias plot and (c) mean vector difference plot for Meteosat-7 IR low level winds for February 2009 compared with the Met Office model background.*

Examination of one case on 26 February at 1800 UTC reveals AMVs of up to 50 m/s assigned to low level with observed minus best-fit pressure differences in excess of 800 hPa (Figure 31).

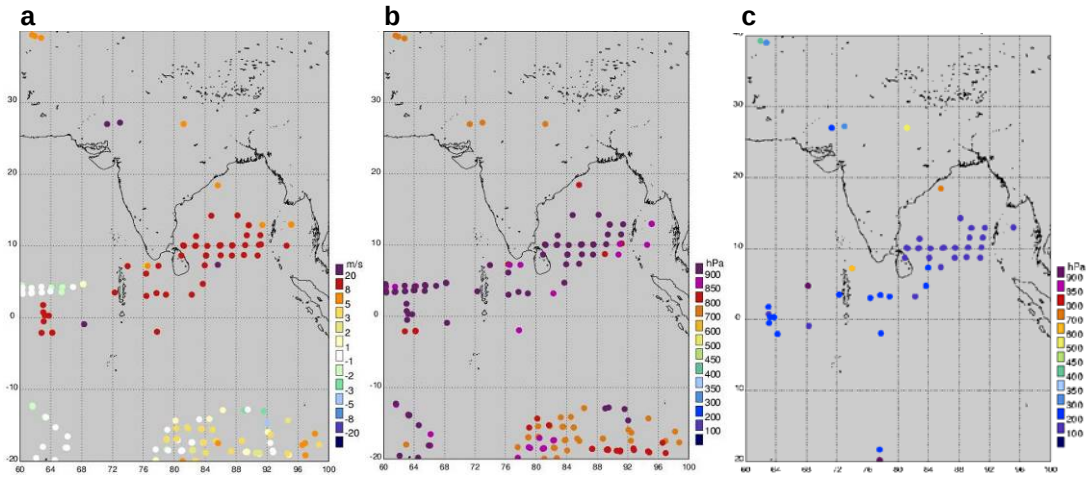

Figure 31: *Visualisation plots showing (a) O-B speed bias compared with the Met Office model background, (b) observation pressure and (c) model best-fit pressure for Meteosat-7 IR low level AMVs valid at 1800 UTC on 26 February 2009.*

MTSAT-1R visible winds show near-neutral bias for most of the year; the main exception is a fast bias off the north-west coast of Australia during September and October. The IR channel, however, exhibits a much greater level of fast bias with considerable variation in the distribution and extent of the bias from month to month. There are three areas that are affected more than others (Figure 32): (A) off the northwest coast of Australia, (B) the South China Sea and (C) a region of Oceania stretching from Indonesia into the west Pacific. The Australian area (A) shows a fast bias for most months of the year, peaking around September and less prominent during May-July. The South China Sea feature (B) is strongest during the summer months May to August.

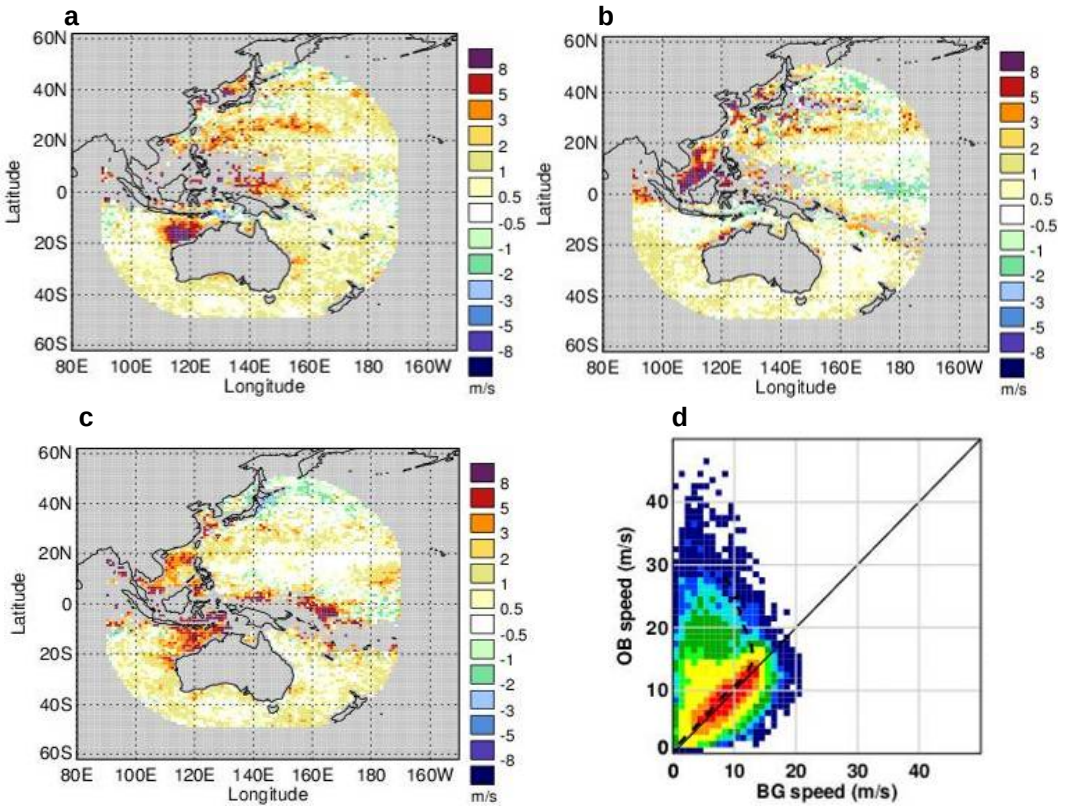

Figure 32: *Map plots of O-B speed bias for low level MTSAT-1R IR winds in (a) September 2008, (b) May 2008 and (c) March 2009 compared with the Met Office model background. (d) Density plot of observed wind speed against Met Office model background wind speed for low level MTSAT-1R IR tropical winds for March 2009.*

The bias in the Oceania region (C) varies in strength from month to month but is particularly prominent in March 2009 for an area 0-15S to the east of the island of New Guinea (see Figure 33c). The affected area coincides with the location of the South Pacific Convergence Zone (SPCZ). This can be distinguished as a band of bright white clouds to the northeast of Australia in the visible satellite image from the 22 March (Figure 33d), when Hovmöller plots show the bias to be particularly strong. The SPCZ is a portion of the ITCZ and forms a band of low level convergence where the northeasterly trade winds to the north converge with the south easterly trade winds to the south. This flow is captured by the model background (Figure 33b) but is less evident in the mean AMV observations (Figure 33a), resulting in a large mean vector difference.

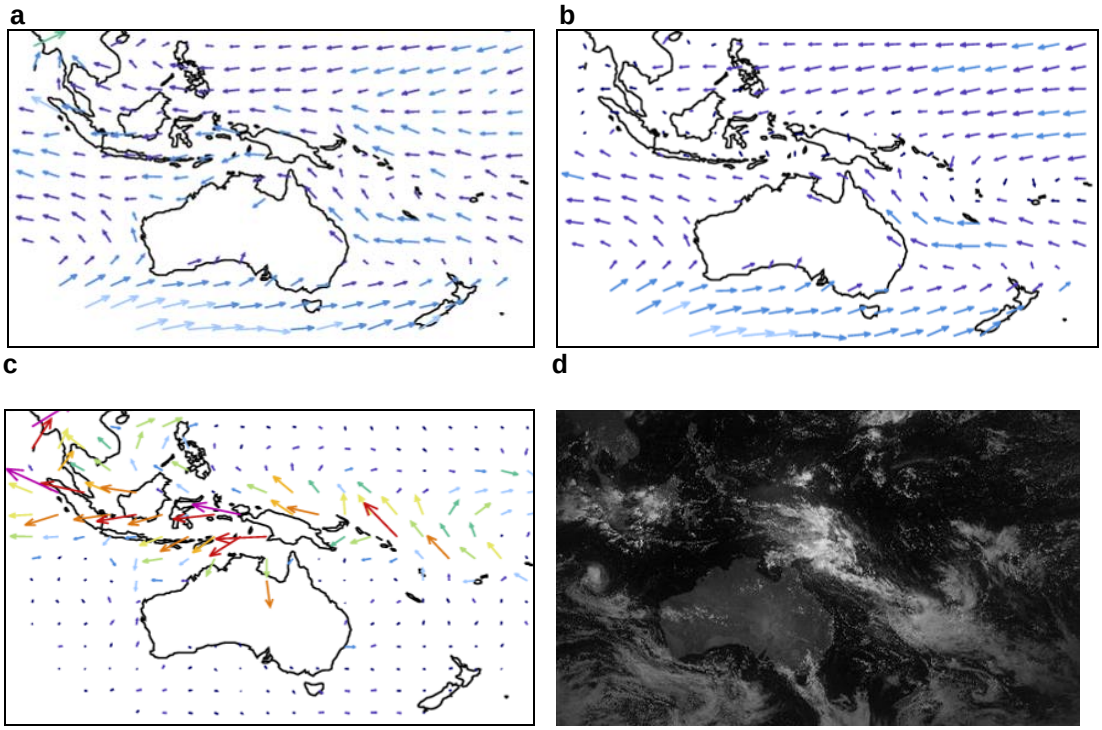

Figure 33: *Vector plots showing (a) the mean observation, (b) the mean background and (c) the mean vector difference for MTSAT-1R IR low level winds compared with the Met Office model background for March 2009. Also, (d) MTSAT-1R visible image for 22 March 2009 0330 UTC.*

The MTSAT-1R O-B bias pattern has been affected by several derivation updates implemented at JMA during 2009:

1. 19 May: improved height assignment scheme for high and mid-level IR AMVs, reducing the target box from 32 to 16 pixels for IR and WV AMVs and an expansion of the derivation region from 50N/S to 60N/S (see http://mscweb.kishou.go.jp/product/product/amv/news/JMA_amv_improvement_May2009.pdf)
2. 18 August: introduction of 3 hourly AMVs
3. 15 September: upgraded tracking algorithm

The impact on the low level statistics is described here; changes at other levels are described in Features 3.1 and 2.10. The 19 May derivation change led to an increased and more widespread fast bias and increased mean vector difference, particularly in the tropics and NH (Figure 34), This was reduced by the derivation change on 15 September 2009. Figure 34 also illustrates the increased latitudinal coverage from 19 May (up to 60N/S) and the increased data volume from 18 August (move to 3 hourly winds).

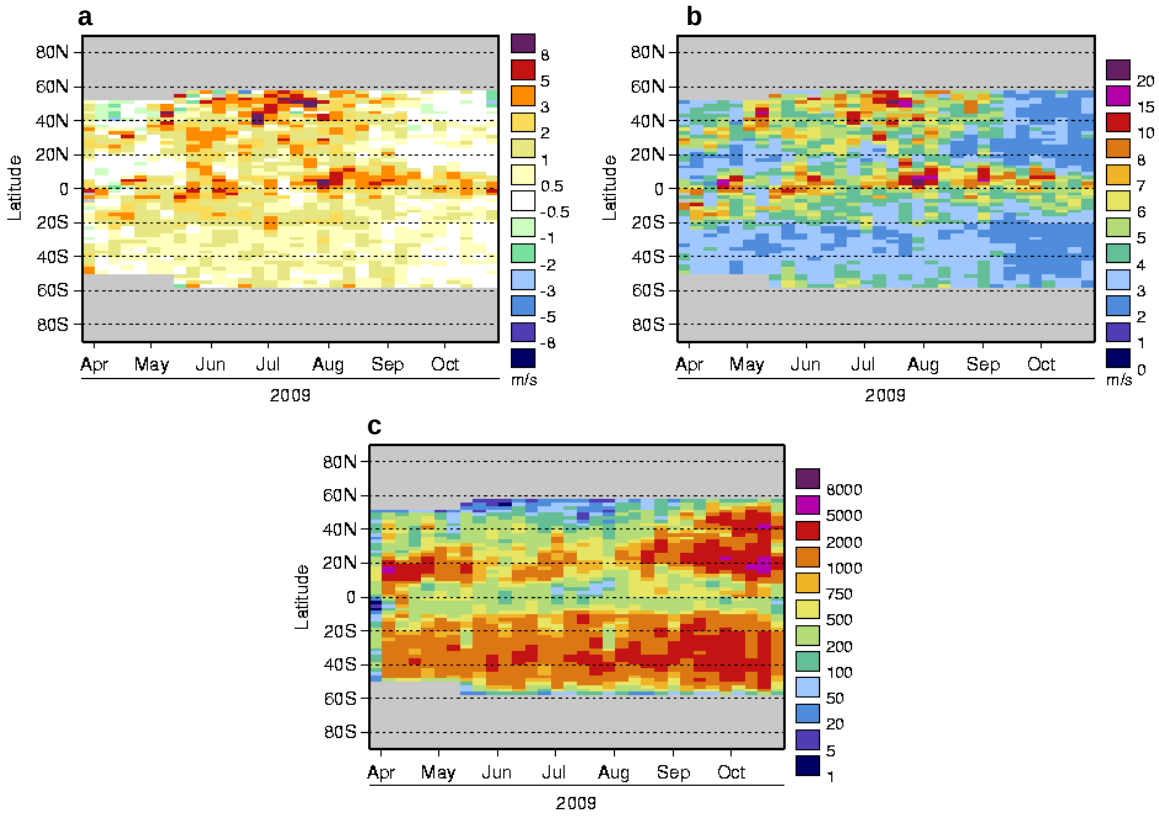

Figure 34: *Hovmöller plots showing (a) O-B speed bias (b) mean vector difference and (c) number of winds for MTSAT-1R IR low level winds compared with the Met Office model background for April-October 2009.*

Feature 4.1 Slow bias in the equatorial Pacific (Met Office plots only)

A slow bias is observed in the equatorial Pacific in the GOES-11 and MTSAT-1R Met Office plots which is not seen in the equivalent plots from ECMWF, as shown by Figure 35. The bias is more marked in the visible channel than it is in the IR and persists, to some extent, for most months of the year. A fast bias is also seen near 15N in the GOES-11 plots from both centres, but is slightly worse in the Met Office plots.

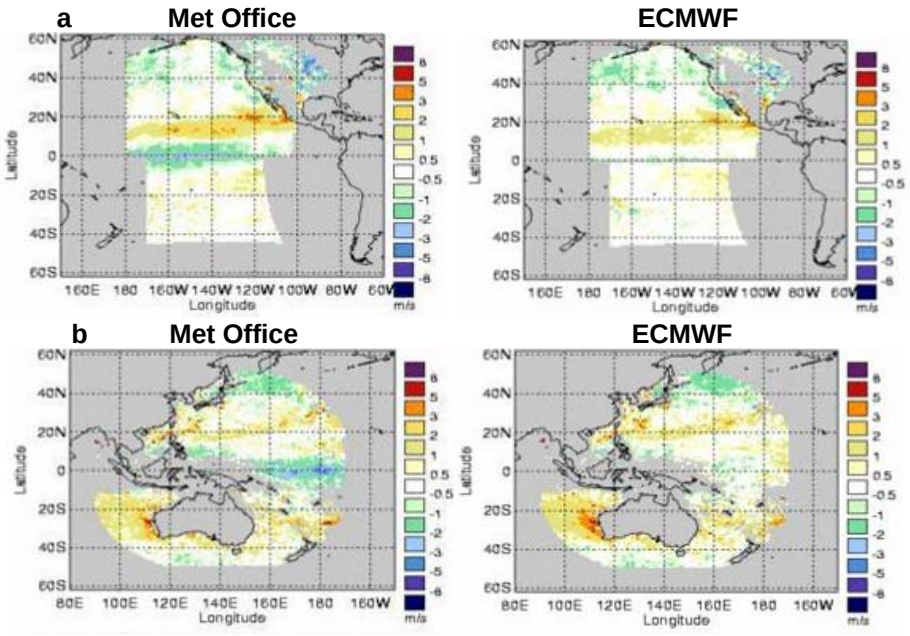

Figure 35: *Map plots of O-B speed bias for (a) GOES-11 VIS AMVs for April 2009 and (b) MTSAT-1R VIS AMVs for February 2009 using the Met Office and ECMWF model backgrounds.*

The maximum easterly equatorial wind is located further south in the Met Office model compared to the observations (Figure 36a) resulting in the paired slow and fast bias at 0 and 15N. The ECMWF model shows better agreement near the equator, but a tendency to be slower than the observations to the north (Figure 36b).

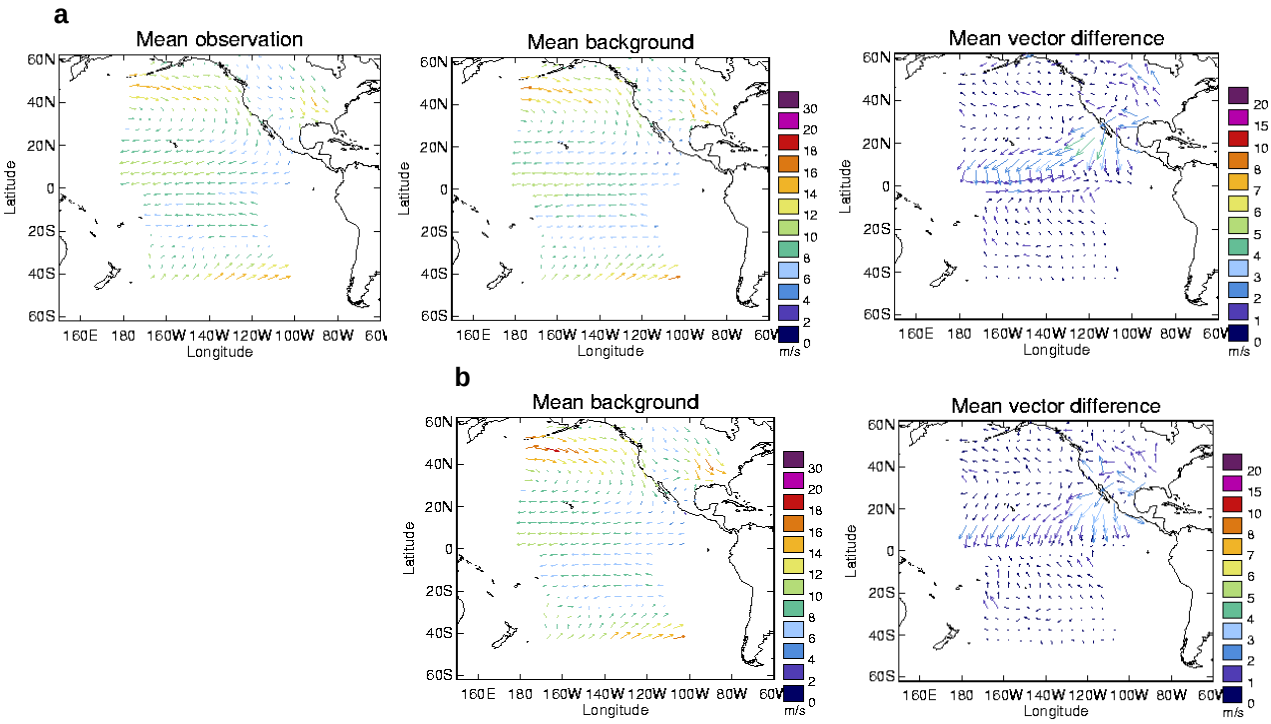

Figure 36: *Vector plots of mean observed vector, mean background vector and mean vector difference for (a) the Met Office and b) ECMWF for low level GOES-11 visible AMVs for April 2009.*

Since the ECMWF plots show very little bias in the equatorial region it is possible the slow bias in the Met Office plots is the result of a bias in the Met Office model and not an issue with the AMVs themselves.

5.3. Mid Level

The mid level wind field is dominated by faster winds beneath the extra-tropical jets (see Figure 22 in the 2nd analysis report). The winds are generally faster than at 850 hPa, but slower than in the jet core between 150-400 hPa. The winds are strongest in the winter hemisphere and show greatest variation in strength in the NH (more land). There are far fewer geostationary AMVs produced at mid level (400-700 hPa) than at high or low levels. Those that are produced generally have poorer O-B statistics, often exhibiting a fast bias in the tropics and a slow bias in the extra-tropics. The poor O-B statistics are thought to result primarily from difficulties with height assignment at these levels.

Update on Feature 2.8. Fast bias in the tropics

A range of tropical mid level fast bias features are described in the 3rd analysis report. These are still evident in more recent monitoring plots. No further analysis has been carried out except for the fast bias feature over the Sahara during the winter months; more details are supplied below.

In the 3rd analysis we described an improvement in the Sahara night-time mid-level fast bias following a EUMETSAT derivation update in March 2007. However a fast bias was still present around 400 hPa during daytime. This is still the case and further investigation indicates that it is associated with winds assigned CO_2 slicing heights (Figure 37).

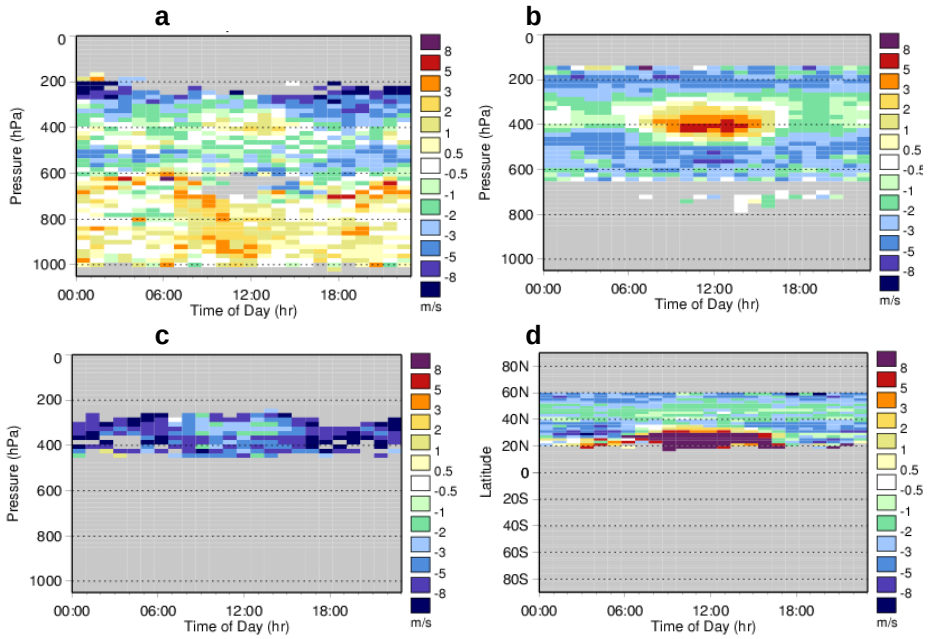

Figure 37: *Hovmöller pressure plots of O-B speed bias as a function of time of day for Meteosat-9 IR 10.8 AMVs compared with the Met Office model background for February 2009 for (a) EBBT, (b) CO_2 slicing and (c) WV intercept height assignment methods. The data was filtered to include only data over land in the NH. Similarly, (d) Hovmöller plot of O-B speed bias over land at mid level assigned using the CO_2 slicing method.*

The fast bias is localised below the sub-tropical jet over the Sahara at 20-30N, where there is large vertical wind shear. One possible explanation is that the speed bias difference is related to a systematic height assignment difference between day time and night time. AMV assigned heights for 0 UTC and 12 UTC on 16 February 2009 (Figure 38) are consistent with this hypothesis, with the night-time heights being higher in the atmosphere and more consistent with other cloud top pressure products. The day time fast bias could point towards an inadequate representation of the large diurnal temperature range of the desert surface, in turn leading to erroneous height assignments. EUMETSAT believe this is related to poor temporal resolution of the forecast surface temperature used in the radiative transfer model (A. de Smet 2009, pers. comm., November 11). This is currently interpolated from a 12-18 hour forecast from ECMWF, but may be helped by using forecast data at 3 hour intervals in the future.

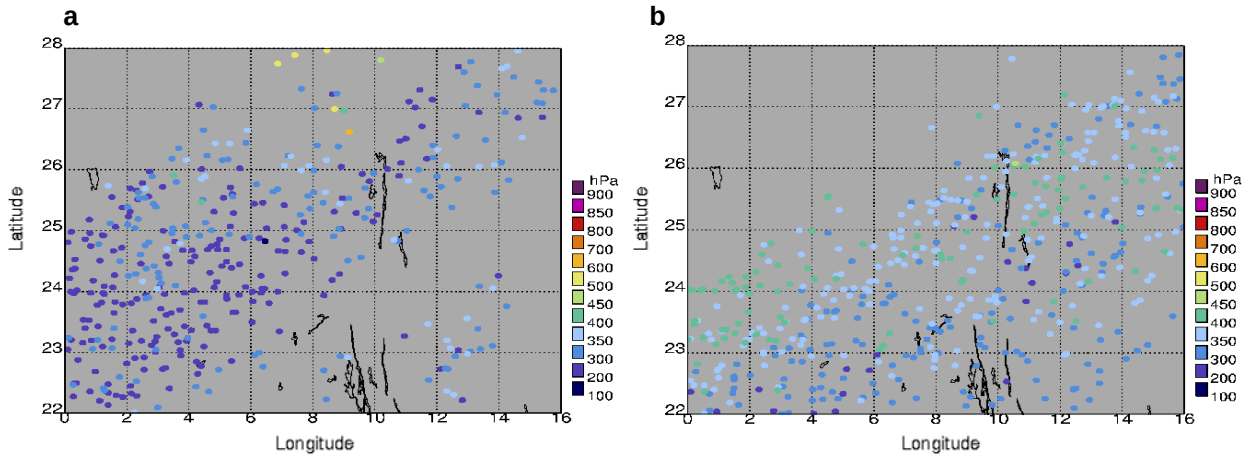

Figure 38: *Plots of Meteosat-9 IR 10.8 AMV height assignment for (a) 2100-0300 UTC and (b) 0900-1500 UTC on 16 February 2009.*

Update on Feature 2.9. Slow bias in extratropics

The extratropics slow speed bias remains prominent in the Meteosat and GOES IR and WV zonal plots. There is a significant seasonal contribution with the bias most marked in the winter hemisphere (Figure 39), except for Meteosat-7 IR winds which exhibit a marked slow bias throughout the year in the SH.

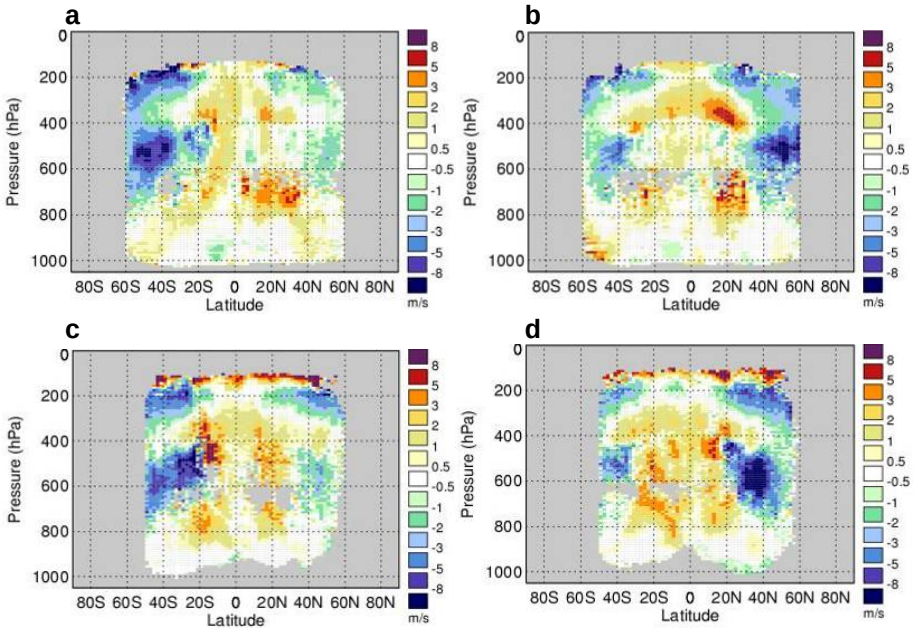

Figure 39: *Zonal O-B speed bias plots compared with the Met Office model background for (a) Meteosat-9 IR 10.8 in June 2009 and (b) November 2008 and (c) unedited GOES-12 IR winds in June 2009 and (d) February 2009.*

In the 3rd analysis report the speed bias was found to be worse for Meteosat-9 winds assigned heights using the CO_2 slicing method and for unedited GOES-12 winds using either CO_2 slicing or WV intercept. This is still the case. It was thought the bias is associated with a high height bias in the model best-fit pressure statistics (see Figure 43 of the 3rd analysis report).

Interestingly Meteosat-8 shows less marked mid level slow speed bias compared with Meteosat-9 (e.g. Figure 40). This, at least in part, relates to more frequent use of EBBT rather than CO_2 slicing for the height assignment of Meteosat-8 mid level winds (discussed in Section 4.3).

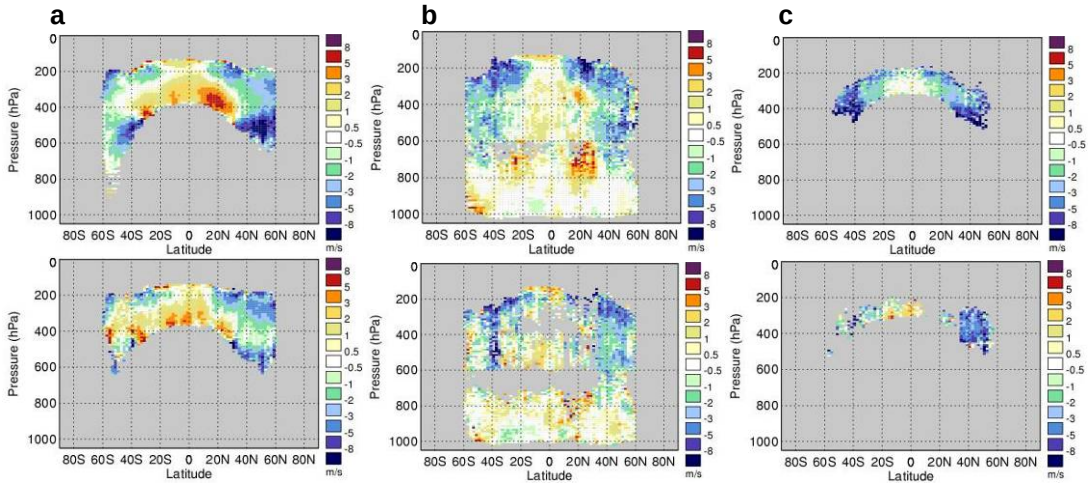

Figure 40: *Zonal O-B speed bias plots for Meteosat-9 IR 10.8 (top) and Meteosat-8 IR 10.8 winds (bottom) compared with the Met Office model background for November 2008 filtered by height assignment method: (a) CO_2 slicing, (b) EBBT and (c) WV intercept.*

The 3rd analysis report showed the model best-fit pressure agreed better with the EBBT pressure than the CO_2 slicing pressure for AMVs below 450 hPa (where the CO_2 slicing method was selected as the final height). This was only investigated for 3 days of data. It is repeated here for the whole month of November 2008. Table 4 shows the effect of varying the pressure threshold. A threshold of 500 hPa shows the biggest

improvement in bias and correlation statistics with respect to the model best-fit pressure. This improvement can also be seen visually in corresponding density plots (Figure 41). If the threshold is decreased to 450 hPa, as in the 3rd analysis report, the density plots (not shown) show improvements in some places, but also a degradation in others and this is reflected in the statistics (near equal correlation).

Minimum Pressure (hPa)	Pressure used	Number	Bias (hPa)	Standard deviation (hPa)	Correlation coefficient
400	CO_2	51620	-21.7	145	0.49
	EBBT	48594	68.0	171	0.22
450	CO_2	15661	-73.0	162	0.40
	EBBT	14896	20.4	163	0.41
500	CO_2	4146	-116.8	166	0.27
	EBBT	3968	-0.8	157	0.45
550	CO_2	1567	-121.6	174	0.18
	EBBT	1521	6.8	164	0.36
600	CO_2	585	-115.4	182	0.11
	EBBT	579	-19.4	166	0.36

Table 4: *Statistics varied by the pressure threshold for winds assigned using the CO2 slicing method: firstly if the CO_2 pressure was used and secondly if the alternative EBBT pressure was used instead.*

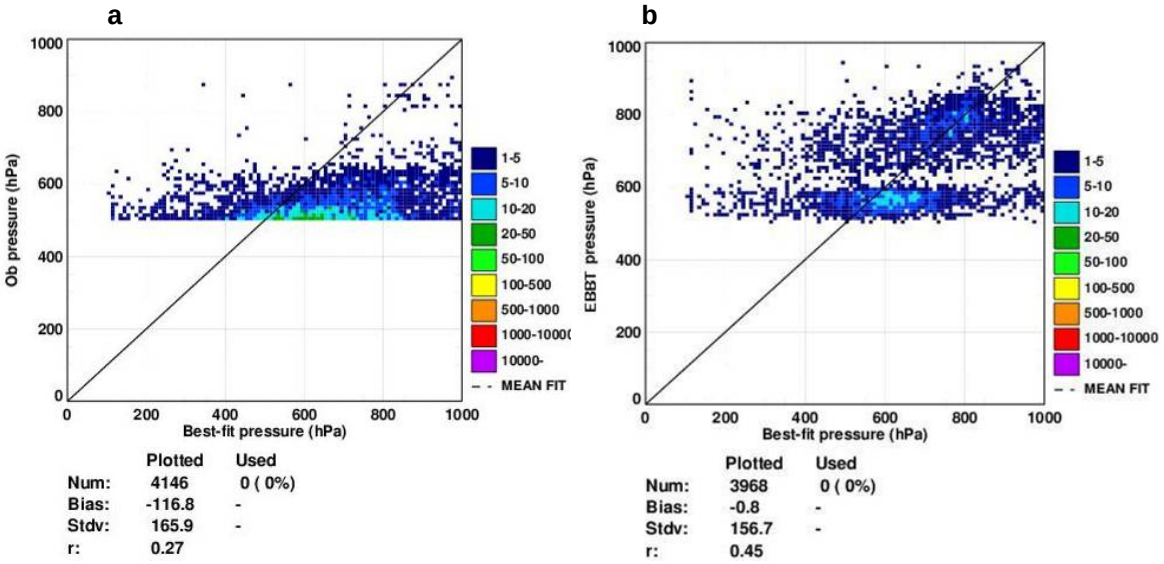

Figure 41: *Density plots and statistics comparing the model best-fit pressure for Meteosat-9 IR 10.8 data in November 2008. The data is filtered to only include winds assigned a height using the CO_2 slicing method below 500 hPa. Plot (a) shows the $C0_2$ slicing pressure and (b) shows the alternative EBBT pressure for these winds.*

These results suggest we may benefit from the application of a 500 hPa pressure threshold, in addition to the existing 253 K temperature threshold. This is under going testing at EUMETSAT. However, the question remains as to why the CO_2 slicing method is systematically putting low levels winds at mid level. A multilayer cloud scenario is one possible explanation.

Update on Feature 3.1. MTSAT-1R mid level fast bias

In the 3rd analysis report a marked fast bias was described for MTSAT-1R winds below ~550 hPa in the atmosphere, which was thought to be linked to a low height bias. An upgrade implemented by JMA on 19

May 2009 (see Feature 2.7 for details) has led to a significant reduction in the bias at mid level (see Figure 42), probably due to improvements to the height assignment scheme.

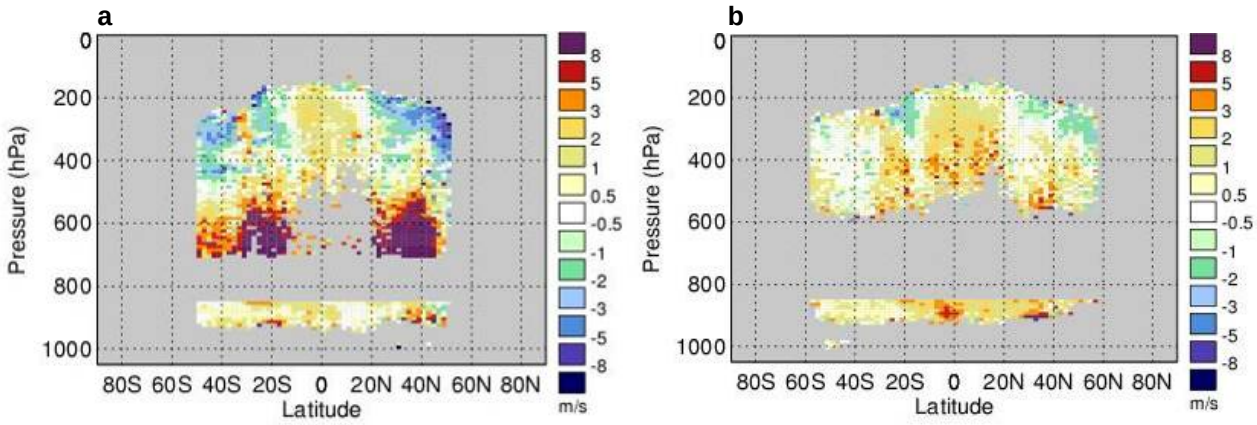

Figure 42: *Zonal O-B speed bias plots for MTSAT-1R IR winds compared with the Met Office model background before and after a derivation change on 19 May 2009: (a) 1-18 May 2009 and (b) 19-31 May 2009.*

5.4. High Level

The high level wind field is dominated by fast winds in the jet regions (see Figure 27 in the 2nd analysis report). The sub-tropical jets are fairly constant westerly flows at around 30S and 30N. The polar front jets are more variable, tend to be more meridional and occur where the polar air meets the warmer air in the mid-latitudes. The two jets in each hemisphere are not always clearly separated and vary in strength and location dependent on the time of year (stronger and closer to the equator during the winter). Nearer the equator, there are some regions of moderate easterlies, particularly over Indonesia, India, the Indian Ocean and Africa. The high level statistics are dominated by a slow speed bias in the jet regions, which is worse in the winter hemisphere. There tends to be a positive speed bias in the tropics, but this is less pronounced than at mid level.

Update on Feature 2.10. Jet Region slow bias

The slow bias in the jet regions has been described in previous NWP SAF analysis reports including some suggestions as to why this occurs. These include:

1. The winds are a spatial and temporal average and therefore will not reflect the strongest winds experienced at a point in space and time.
2. The AMVs represent the motion of a layer, but are currently assigned to a single height.
3. The clouds are typically located below or to the side of the high speed jet core and so will not reflect the highest wind speeds.
4. The wind may blow through the tracer and therefore the tracer is no longer representative of the wind speed.
5. There maybe a systematic height assignment error.

The slow bias is known to be associated with the jet regions and is most prominent in the winter months when the jets are at their strongest. In the 3rd analysis it was noted that MTSAT-1R IR winds exhibited some of the largest biases of the different satellite-channel combinations. Figure 43 compares bias plots for MTSAT-1R IR high level winds for July 2008 and July 2009. The jet slow bias is much reduced in July 2009.

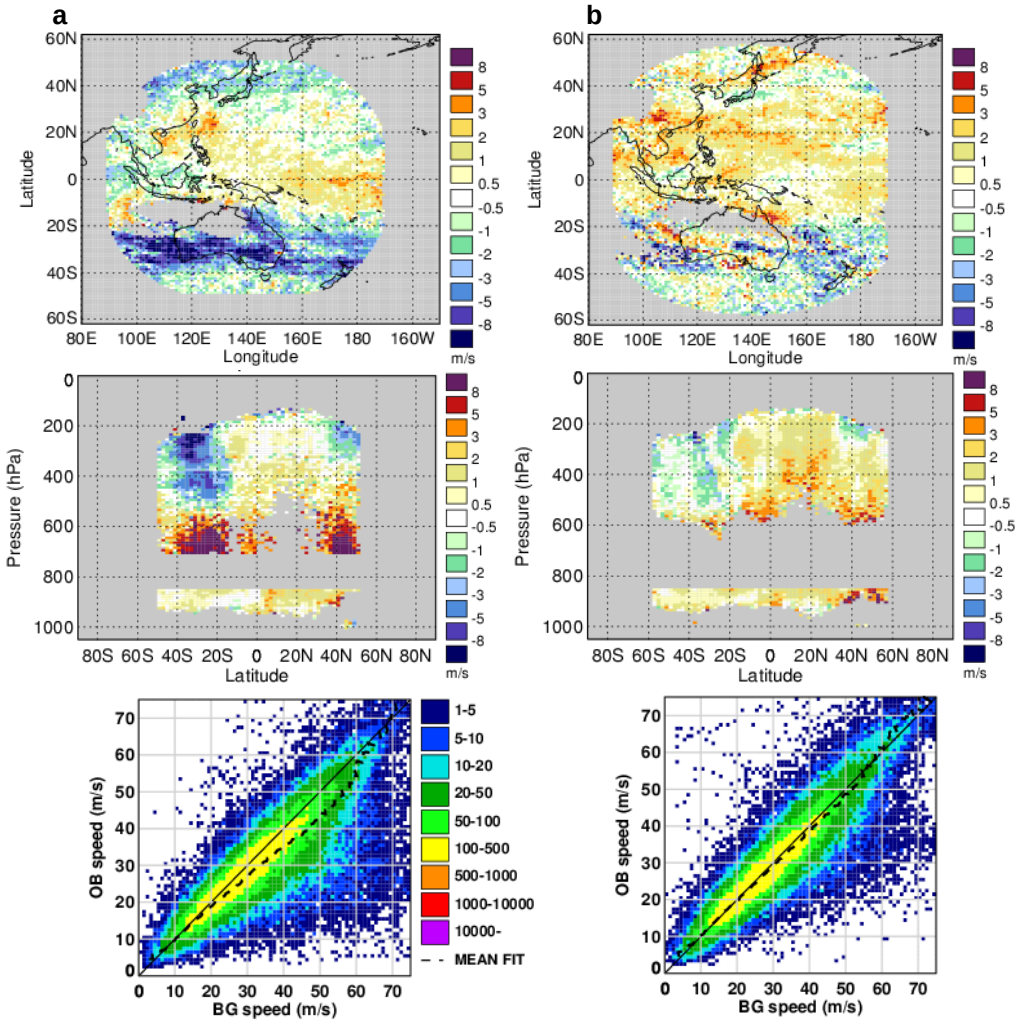

Figure 43: *Map (high level) and zonal plots of O-B speed bias compared with the Met Office model background for MTSAT-1R IR for (a) July 2008 and (b) July 2009. Also, density plots of observed wind speed against the Met Office model background for high level winds in the SH for the same months.*

This improvement followed the 19 May 2009 JMA derivation change which included an improved height assignment scheme and reduced target box size (see Feature 2.7 for further details). Whilst the IR jet slow bias is reduced, there is a tendency for the fast bias to worsen. This is apparent in the tropics for the IR high level plots (Figure 43), but is most marked for the WV channel. In this case the fast bias, which is anyway worse, becomes more widespread, even extending into the jet regions (e.g. Figure 44).

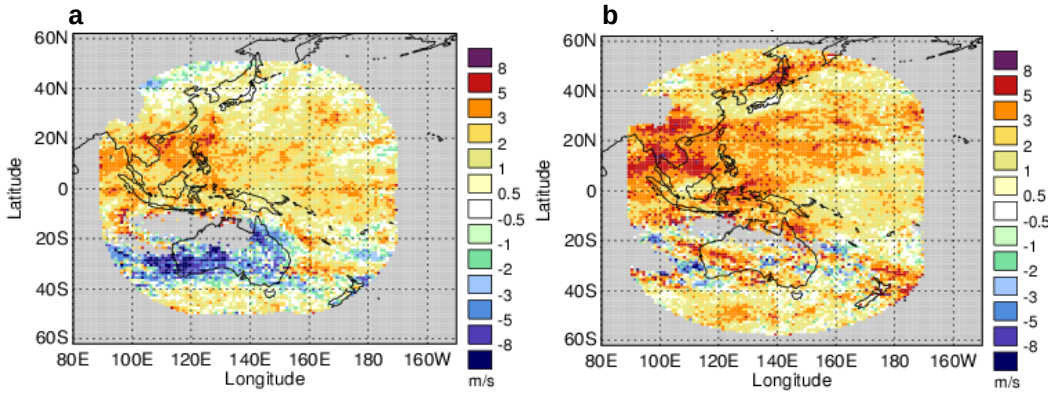

Figure 44: *Map plots of O-B speed bias compared with the Met Office model background for high level MTSAT-1R WV for (a) July 2008 and (b) July 2009.*

The worsening in fast bias for the IR and WV channels is reduced by the 15 September 2009 JMA derivation change (see Figure 45).

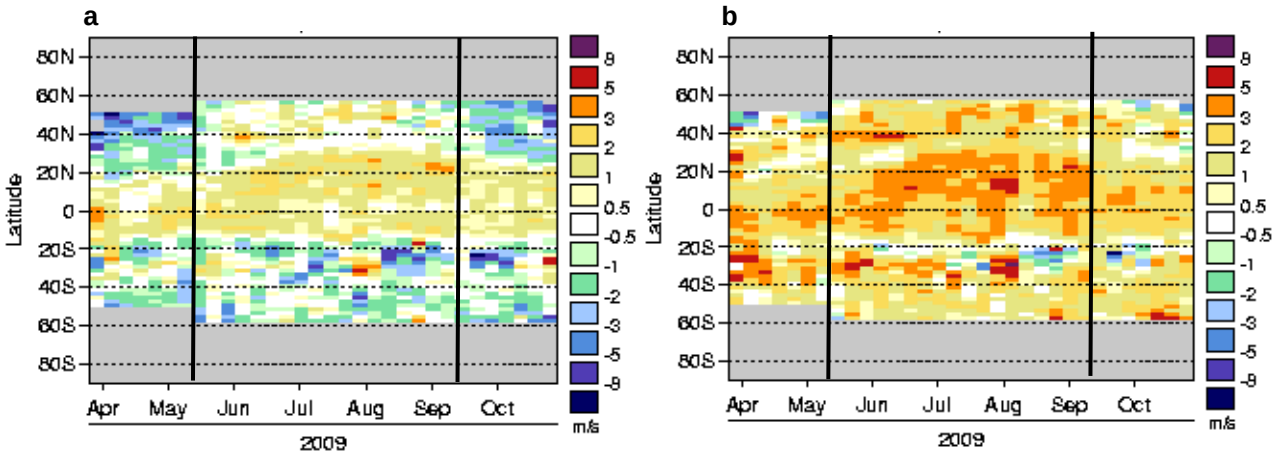

Figure 45: *Hovmöller plots of O-B speed bias compared with the Met Office model background for (a) high level MTSAT-1R IR and (b) high level MTSAT-1R WV for April-October 2009. Black lines mark the JMA May and September change dates.*

To improve our understanding of the jet region slow bias we can investigate individual cases. One fairly persistent feature is a large swathe of slow bias for Meteosat-7 WV AMVs over the Indian Ocean, stretching from Madagascar to Western Australia (Figure 46), which is also observed in the Meteosat-7 IR and Meteosat-9 WV and IR plots. The bias is most prominent during May to September (SH winter), particularly in the region of the sub-tropical jet at around 20-30S (Figures 46b and c) but is also seen in the region of the polar front jet at around 45S in the SE Indian Ocean.

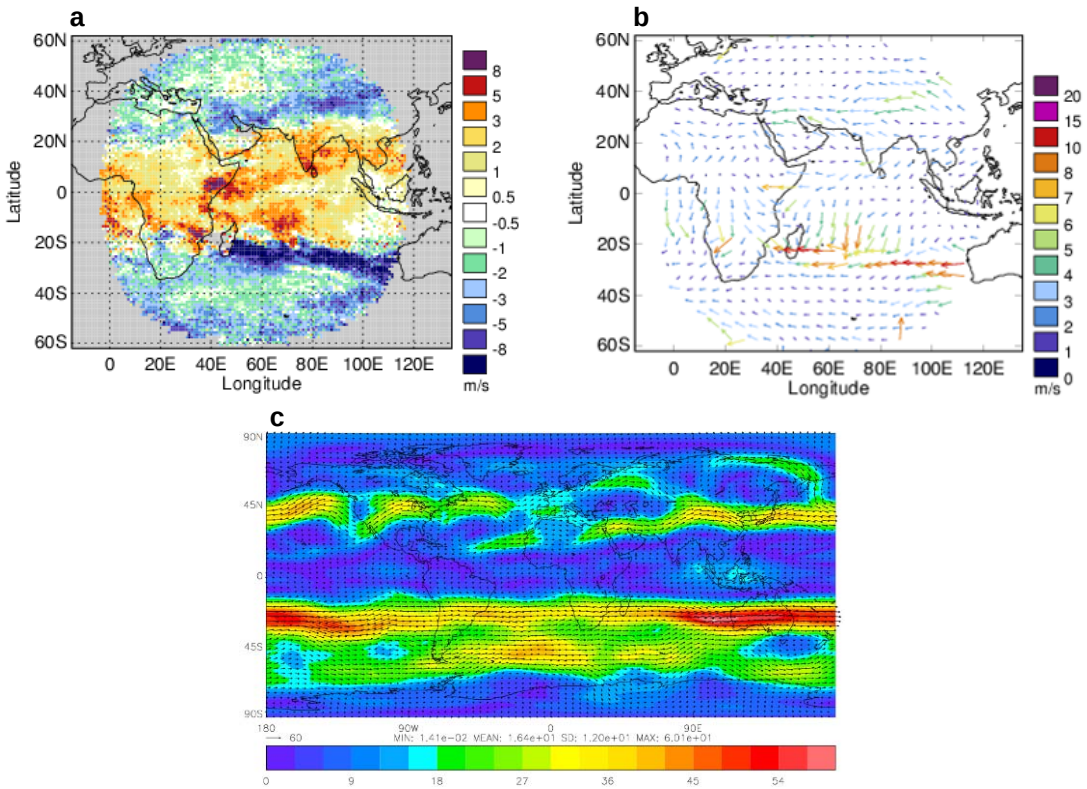

Figure 46: *Met 7 WV June 2009 Map plots of (a) O-B speed bias and (b) mean vector difference for June 2009 compared with the Met Office model. (c) Mean Met Office 250 hPa analysis wind speed (colours) and vectors (arrows) for June 2009.*

Figure 47 shows how this feature varies in magnitude from day to day. The largest biases associated with both jet regions coincide to some extent, but not exclusively, with the fastest model wind speeds. For example, there is a good relationship between the slow bias and stronger wind speeds around 50-60S for the period 18-23 June, but the bias is not apparent at 20-30S for 12-16 June, when the model speeds are again strong.

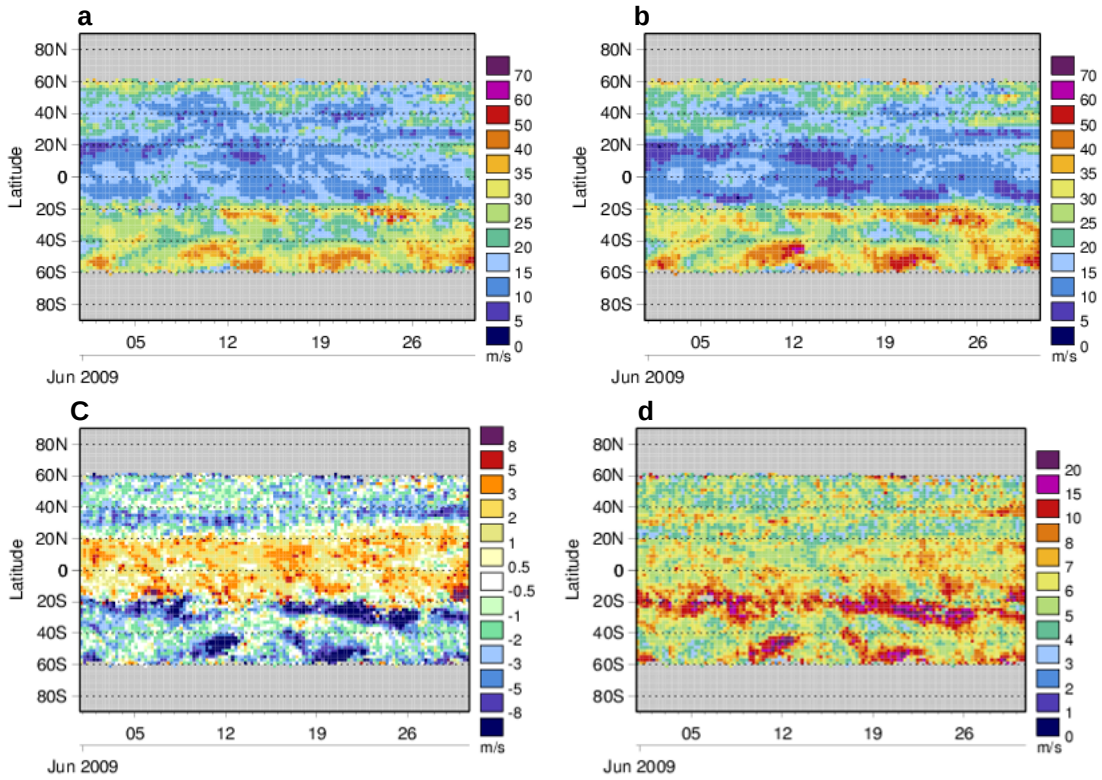

Figure 47: *Hovmöller plots of (a) mean observation speed, (b) mean background speed, (c) O-B speed bias and (d) mean vector difference for June 2009 for Meteosat-7 WV compared with Met Office model background.*

Visualisation of the data can be used to investigate further. Examples are shown here for 22 and 29 June 2009. On the 22 June 2009 the sub tropical jet is observed near 25S to the West of Australia with the polar front jet closer to the pole at 50S. Both jets exhibit AMVs with wind speeds in excess of 70 m/s or 136 knots (Figure 48b) and are associated with large slow biases (dark blue points in Figure 48a).

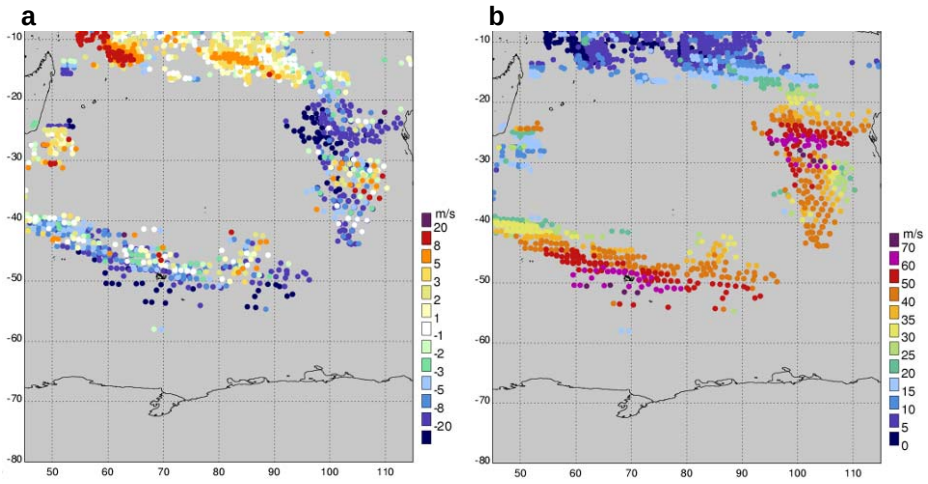

Figure 48: *Visualisation of (a) O-B speed bias compared with the Met Office model and (b) model background wind speed for high level Meteosat-7 WV AMVs valid at 00 UTC 22 June 2009.*

The 29 June 2009 case is less straightforward (Figure 49). There are fast winds to the west of Madagascar and a cluster around 105E, 35S which as before are considerably slower than the model background winds. However, for a large section of the jet centred around 55E, 40S the AMVs show more neutral bias or in some cases fast bias compared to the model. The question is why are large slow biases associated with very fast winds on some occasions and not others? Looking at the satellite imagery may provide some clues.

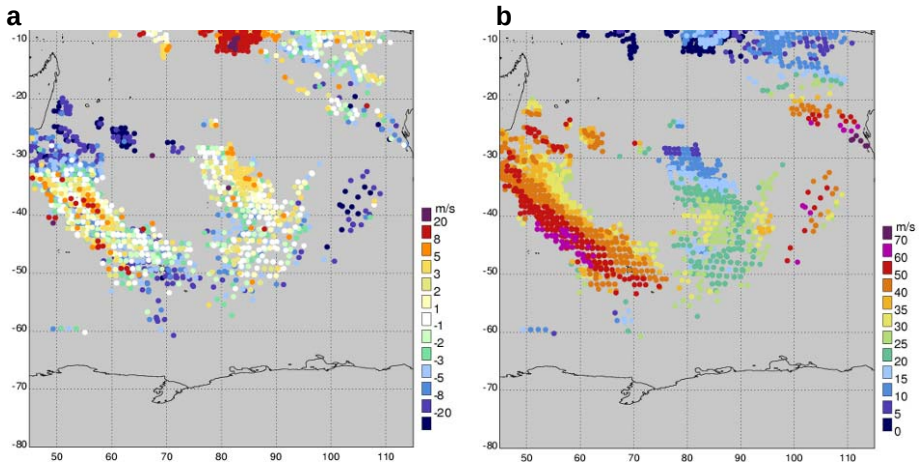

Figure 49: Visualisation of (a) O-B speed bias compared with the Met Office model and (b) model background wind speed for high level Meteosat-7 WV AMVs valid at 00 UTC 29 June 2009.

Figure 50 shows Meteosat-7 WV imagery for the two cases on the 22 and 29 June. Some features of interest are indentified via labels 1 to 4. Feature 1,3 and 4 correspond to jet regions which exhibit fast winds with a significant slow bias. Feature 2 highlights a region of jet strength winds, but where there is more neutral bias. Visually the key difference between the examples is the shape and texture of the WV features in the imagery. Features 1, 3 and 4 are relatively narrow jets with smooth linear features within the jet core aligned parallel to the direction of motion. Contrast this with feature 2 which is much wider, with much less regular texture and some contrast details running perpendicular to the flow direction. Without examining individual targets it is hard to be certain, but the differences in texture may affect the success of the tracking, with increased biases when the imagery is more smooth and linear. Considering the 29 June case it is interesting to note that the model background wind is of similar strength in Features 2 and 3, whereas the observed speed is much less in Feature 3. If we believe the model winds this suggests that the bias, at least in this case, is a result of the tracking step rather than the height assignment.

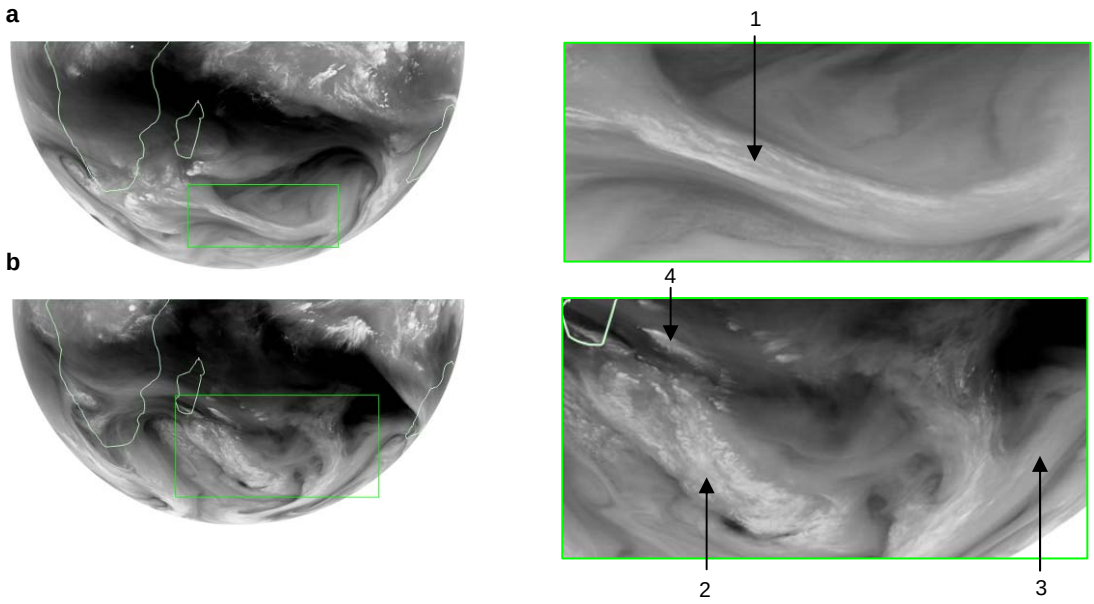

Figure 50: *Meteosat-7 WV imagery for (a) 00 UTC 22 June 2009 and (b) 00 UTC 29 June 2009, showing the SH disc and also cropped to the area of interest.*

Update on Feature 2.13. Tropics fast bias

A fast speed bias is observed at high levels in the tropics for most satellite-channel combinations but tends to be more marked in the WV channels. A small fast bias persists in the tropics throughout the year but some areas are more affected than others (see Table 5 and examples in Figure 51).

Region of bias	Satellites affected	Peak period
10-20S in Atlantic	Meteosat-9	July-November
~20N in Atlantic	Meteosat-9, unedited GOES-12	February-April
Indian Ocean and East Africa	Meteosat-7, Meteosat-9	June-September (SW monsoon)
SE Pacific at 0-20S	Unedited GOES-12	All year, peaks July-August

Table 5: *Table highlighting the main areas of fast bias at high level*

In addition to the examples in Table 5, the MTSAT-1R WV AMVs show a widespread fast bias. These are not pursued further here as the characteristics have changed following recent derivation changes (see Feature 2.10) and we have insufficient data to identify new trends.

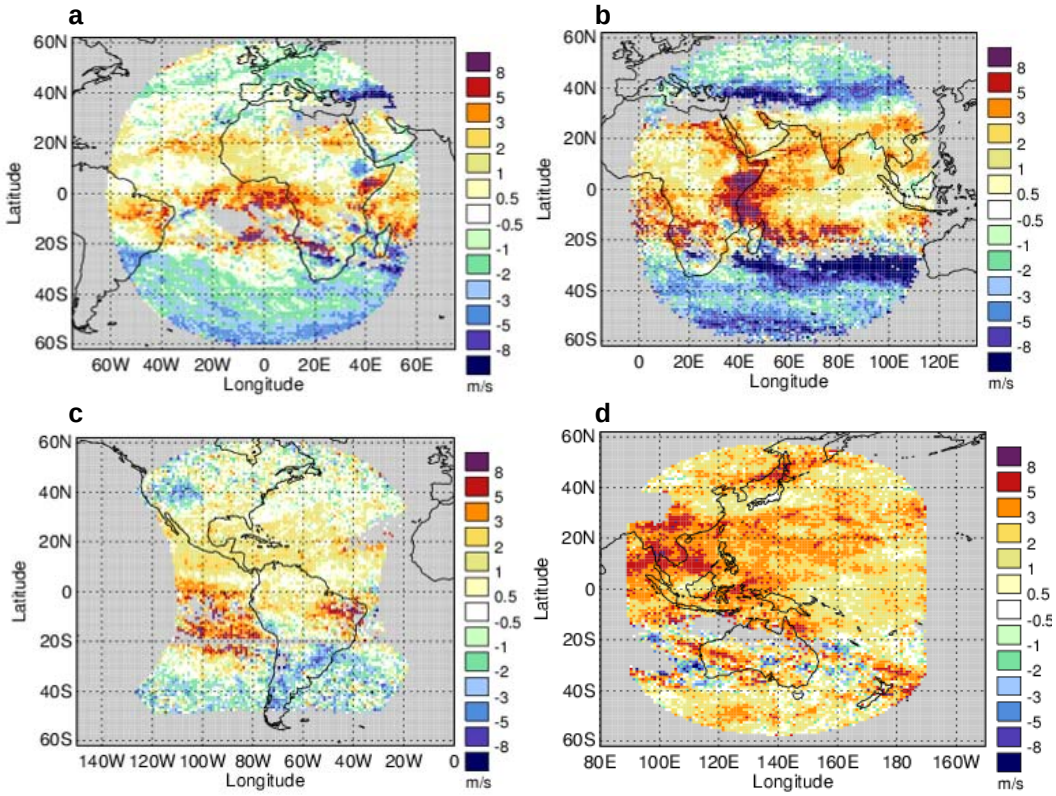

Figure 51: *Map O-B speed bias plots for high level winds from (a) Meteosat-9 IR 10.8 (b) Meteosat-7 WV, (c) unedited GOES-12 WV and (d) MTSAT-1R WV for July 2009.*

Hovmöller plots (not included) show that the high level fast bias varies from day-to-day. On further investigation many relate to fairly isolated linear cloud features. Examples are provided below:

A prominent fast bias around 20S in the Atlantic on 17 November 2008 is associated with a linear cloud feature oriented NW-SE (Figure 52). This feature is located away from the main cloud areas of the ITCZ and jet regions. This is similar to a case identified in the 3rd analysis report (see Figure 51 3rd analysis report).

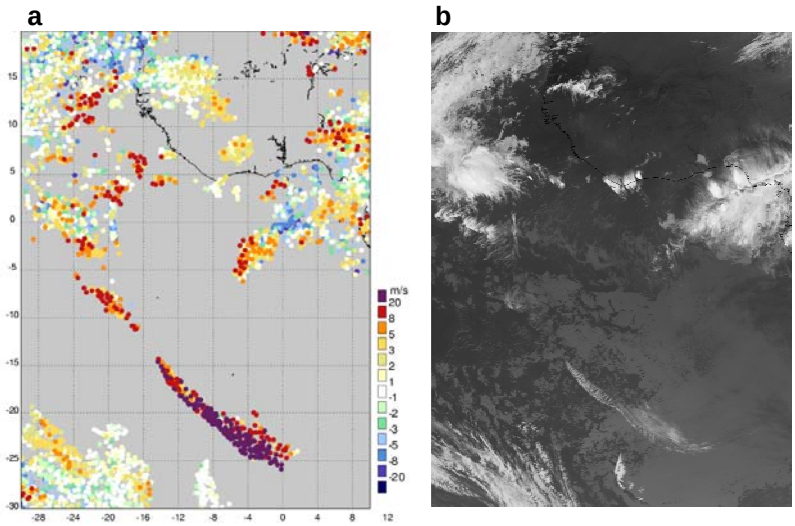

Figure 52: *(a) Visualisation of O-B speed bias compared with the Met Office model for high level Meteosat-9 IR10.8 AMVs valid at 1800 UTC 17 November 2008. (b) Meteosat-9 IR10.8 image for 1815 UTC 17 November 2008.*

Figure 53 shows the development of this cloud feature in the IR satellite imagery over 6 hours. The initial growth of the cloud occurs towards the northwest. It then broadens and develops along its length from northwest to southeast as indicated by the red arrows, before peaking in size and definition at ~1800 UTC.

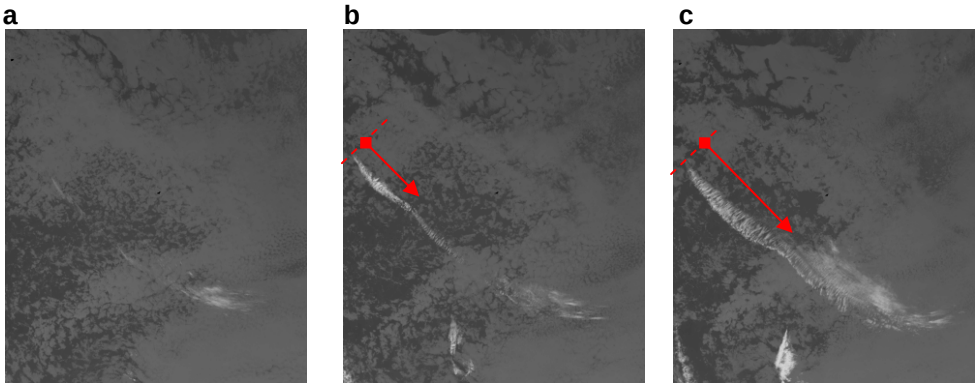

Figure 53: *Meteosat-9 IR10.8 image sequence of a linear cloud feature over the Atlantic centred around 20S, 8W for (a) 1215 UTC (b) 1515 UTC and (c) 1815 UTC 17 November 2008.*

The development of the cloud during the 6 hr period may contribute to the observed fast bias, particularly in the NW section. However, it is likely the height assignment also contributes to the error as CALIPSO cloud top heights (Figure 54) and model best-fit pressure (Figure 55b) are consistent with a level around 200 hPa.

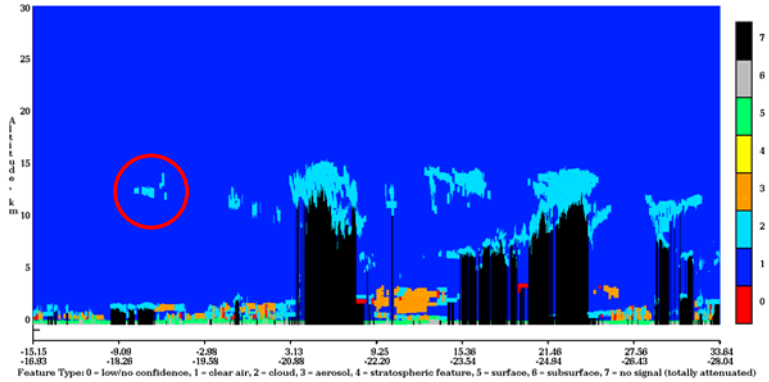

Figure 54: *CALIPSO vertical feature mask for 1503 UTC on 17 November 2009. The circle marks the cloud feature of interest.*

The AMV assigned pressures are mostly lower, particularly in the SE section (see Figure 55a). It is possible the heights (mostly CO_2 slicing) are affected by multi-level cloud (as apparent in the satellite imagery). In cases of high level semi-transparent cloud overlying lower level cloud, most height assignment methods will put the cloud part way between the two. Interestingly the WV 6.2 intercept methods provide pressures in better agreement with the model and CALIPSO for this case (e.g. Figure 55c), probably as this channel is less sensitive to the lower level cloud.

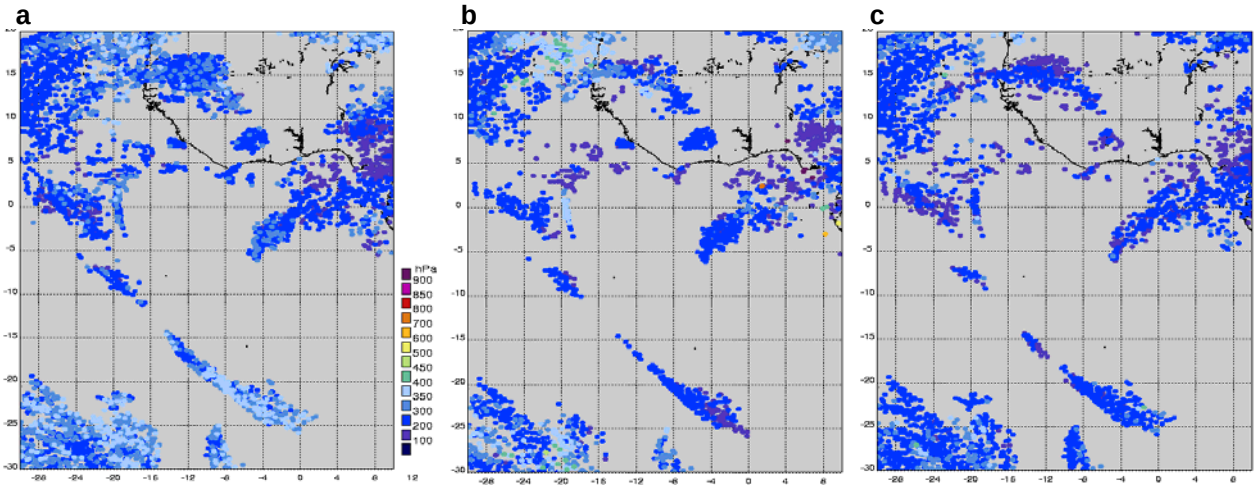

Figure 55: *Plots of (a) observed pressure, (b) model best-fit pressure and (c) alternative semi-transparent correction WV 6.2 pressure for data valid at 1500-2100 UTC on 17 November 2008.*

A fast bias is also sometimes observed in the Meteosat-9 and unedited GOES-12 plots around 20N in the Atlantic, where it generally forms a narrow feature (e.g. Figure 56).

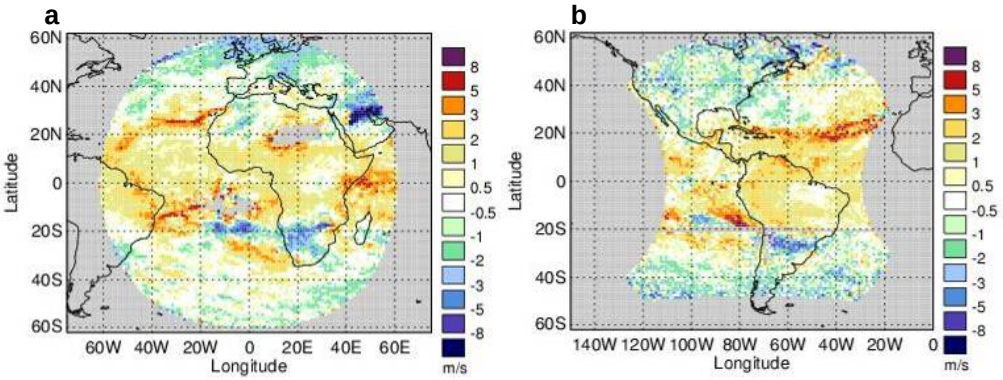

Figure 56: *Map O-B speed bias plots for (a) Meteosat-9 WV 7.3 in October 2008 and (b) unedited GOES-12 WV winds in April 2009 compared with the Met Office model background.*

The Hovmöller plot for October (Figure 57) shows that the bias near 20N was particularly prominent for a couple of days at the end of the month.

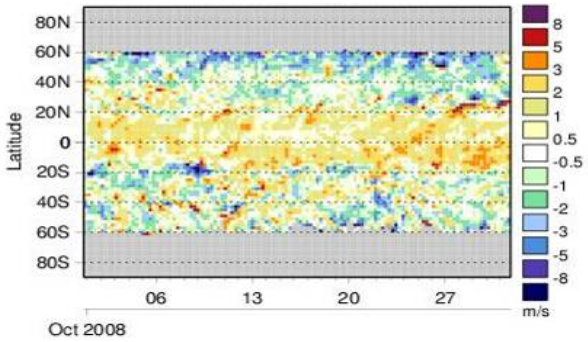

Figure 57: *Hovmöller plot of O-B speed bias for Meteosat-9 WV 7.3 high level winds compared with the Met Office model background in October 2008.*

For a case at 1800 UTC on 28 October 2008, the fast bias feature (which exceeds 20m/s) spans the Atlantic Ocean (Figure 58a) and is associated with an arc of high level cloud (Figure 59a). The fast bias is worst for AMVs along the northern edge of the cloud where the observed wind speed is in excess of 40m/s (Figure 58d). The bias is likely due to AMVs being put slightly too low in an area of high vertical wind shear (Figures 58c and e). A similar example in Galante Negri and Forsythe (2009) was explained by the use of EBBT height assignment for the problem winds. However, in this case the CO_2 slicing method is used for most winds (Figure 58f). The CALIPSO cloud feature mask in Figure 59b for a pass through the same cloud earlier in the day shows that its northern edge is where the cloud is thinnest and lies above a band of broken low cloud. In these multi-level cases, the height assignment will tend to be put somewhere between the cloud layers and could explain the pressure bias seen between the AMVs and model best-fit pressure.

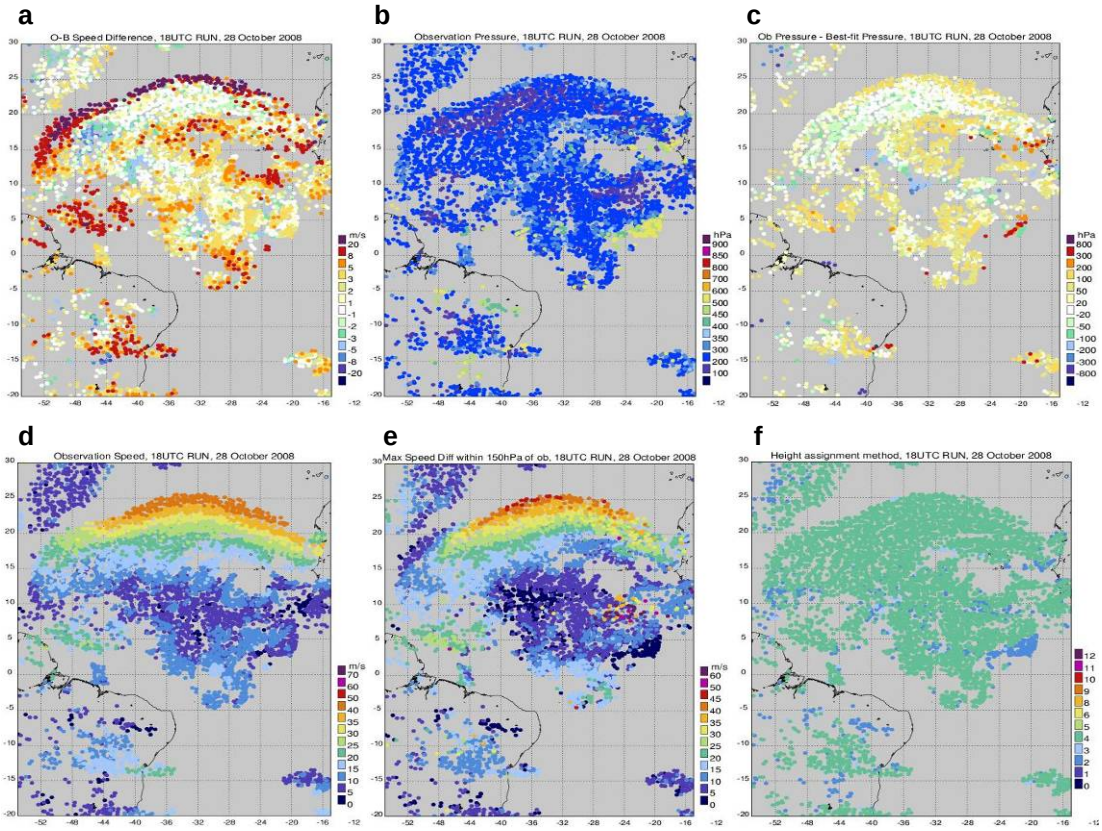

Figure 58 *Visualisation plots showing (a) O-B speed bias compared with the Met Office model background, (b) observation pressure, (c) observed minus model best-fit pressure, (d) observation speed, (e) maximum speed difference within 150 hPa, (f) height assignment method for Meteosat-9 WV 7.3 winds valid at 1800 UTC on 28 October 2008.*

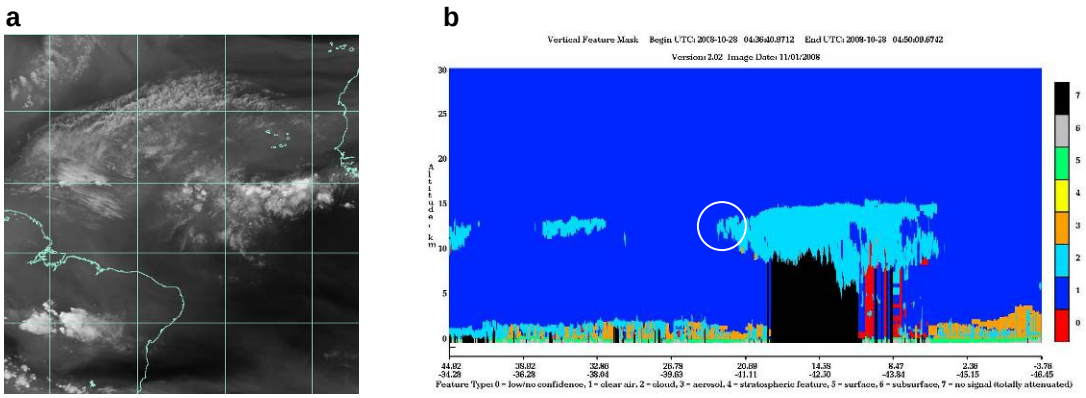

Figure 59: *(a) Meteosat-9 WV 6.2 image for 1800 UTC on 28 October, Copyright 2008 EUMETSAT/Met Office. (b) CALIPSO cloud feature mask for 0436 UTC on 28 October 2008 with the north edge of the cloud of interest circled. Source: NASA.*

To understand what is happening at the synoptic scale we can look at plots of 200hPa streamlines for the tropical and central North Atlantic (Figure 60). From this we can identify a Tropical Upper Tropospheric Trough (TUTT) as demonstrated by the trough axis line drawn in blue. These troughs are major features of the upper level circulation (around 200hPa) of the North Atlantic and extend across the entire ocean from NE to SW. TUTTs usually form as a result of an intrusion of energy into the tropics from the mid latitudes but are normally associated with the summer months. As shown by Figure 60b the trough axis matches up well with the WV feature being tracked by the AMVs. Strong TUTTs can bring significant vertical wind shear into the tropics as indicated in this case by Figures 60c and 60d.

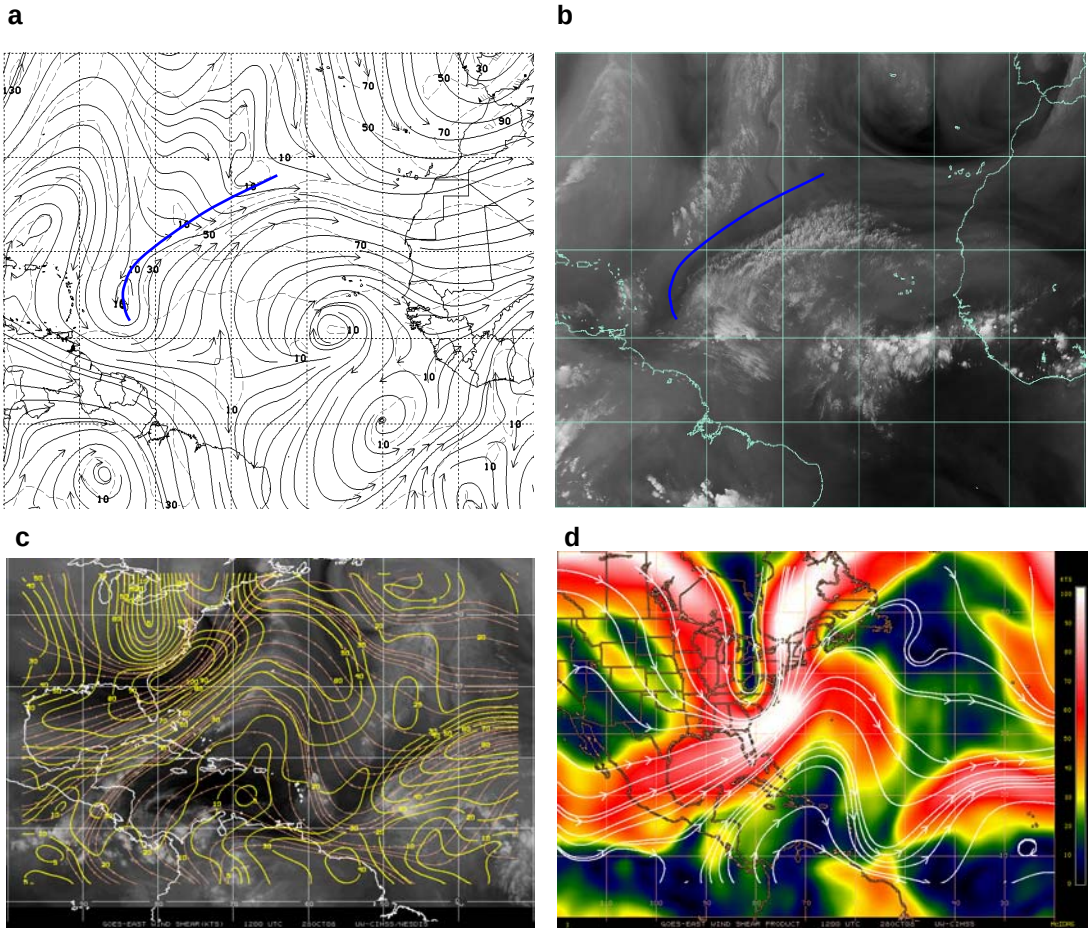

Figure 60: *(a) 200 hPa streamlines (NOAA/Tropical Prediction Centre Miami Fl) and (b) Meteosat-9 WV 6.2 image for 1800 UTC on the 28 October (Copyright 2008 EUMETSAT/Met Office). The approximate location of the TUTT axis has been added by hand. Also, deep layer wind speed shear (c) displayed over a satellite image background and (d) colour contour plot (both University of Wisconsin – CIMSS). The contours show the vector magnitude shear (absolute value) and the streamlines indicate the direction of the shear. Both (c) and (d) are generated by CIMSS using the gridded AMV output u and v components averaged over an upper layer (150, 200, 250, 300, and 250 hPa) and a lower layer (700, 775, 850, and 925 hPa). The difference between upper and lower layers is used to compute the wind speed shear.*

Note that the fast bias on 28 October is also observed in the Meteosat-9 IR channel and the unedited GOES-12 WV channel (Figure 61), although in the GOES case the bias is not present to the east of 44W where the AMVs associated with the very northern edge of the cloud are not present, probably due to stricter quality control at NESDIS.

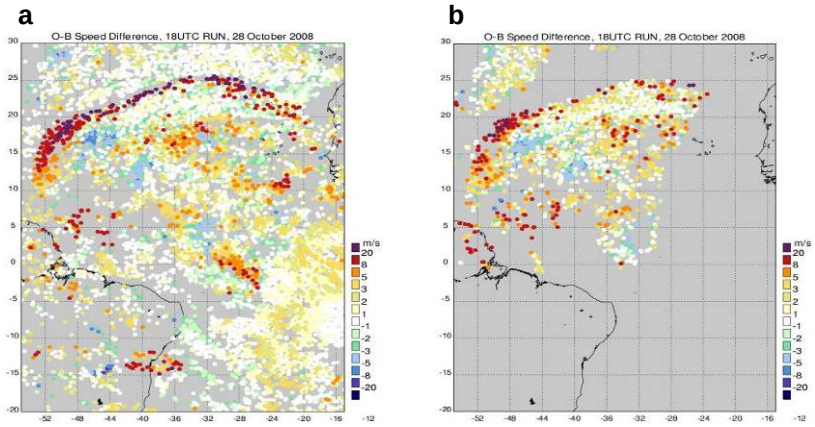

Figure 61: *Visualisation plots showing O-B speed bias compared with the Met Office model background for (a) Meteosat-9 IR 10.8 and (b) unedited GOES-12 WV winds valid at 1800 UTC on 28 October 2008.*

To understand how typical the case on 28 October 2008 is, other cases were examined on 7 February 2009 (Figure 62) and 25 April 2009 (Figure 63). These show very similar bias patterns with the fast bias most prevalent along the northern edge of the cloud.

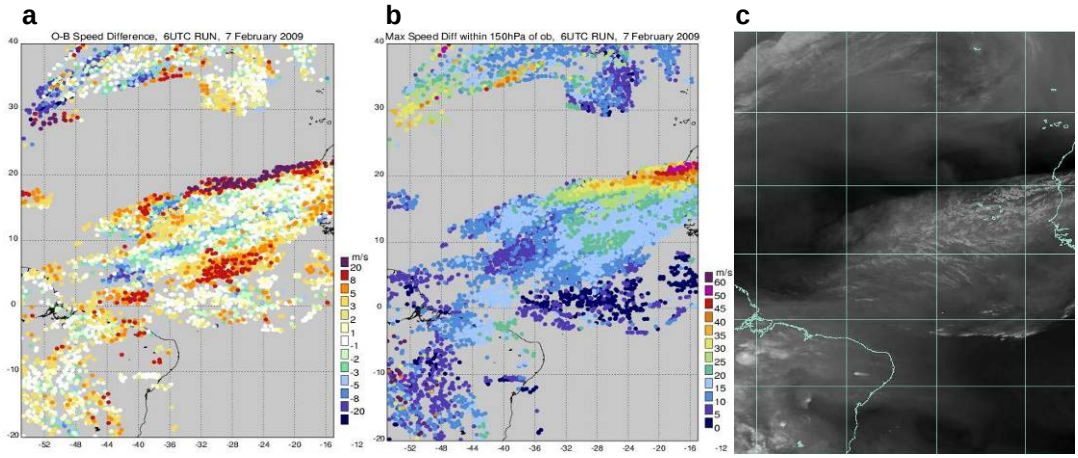

Figure 62: *(a) O-B speed bias compared with the Met Office model background, (b) maximum speed difference within 150 hPa for Meteosat-9 WV 7.3 winds valid at 0600 UTC on 7 February 2009. c) Meteosat-9 WV 6.2 image for 0600 UTC 7 February 2009, Copyright 2009 EUMETSAT/Met Office.*

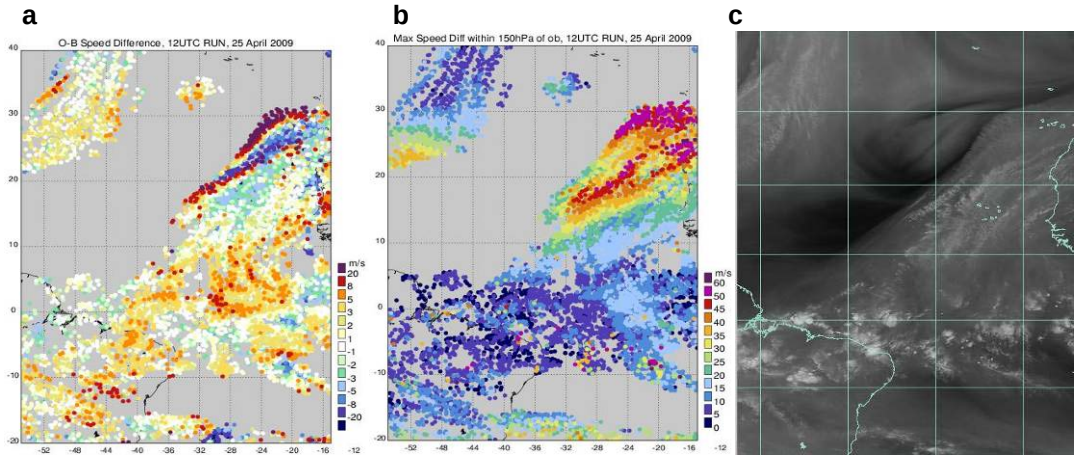

Figure 63: *(a) O-B speed bias compared with the Met Office model background, (b) maximum speed difference within 150 hPa for Meteosat-9 WV 7.3 winds valid at 1200 UTC on 25 April 2009. (c) Meteosat-9 WV 6.2 image for 1200 UTC 25 April 2009, Copyright 2009 EUMETSAT/Met Office.*

An example on 8-9 April 2009 shows this type of bias is not confined to the northern edge of cloud as seen thus far. For AMVs valid at 1200 UTC on 8 April 2009 the fast bias looks familiar to the cases already seen with the bias located along the northern edge of a cloud (Figure 64a). However by 1200 UTC on 9 April the feature has evolved into more of a 'wave' shape with a fast bias also present on the southern edge even though the wind shear is much less (Figures 64b and c). Figure 65 shows the CALIPSO feature mask for a satellite pass around 1600 UTC on the 9 April which reveals a complicated multilayer scenario with a wide band of thin, high-level cloud (10S-10N) overlying clouds in the convergence zone (~3S).

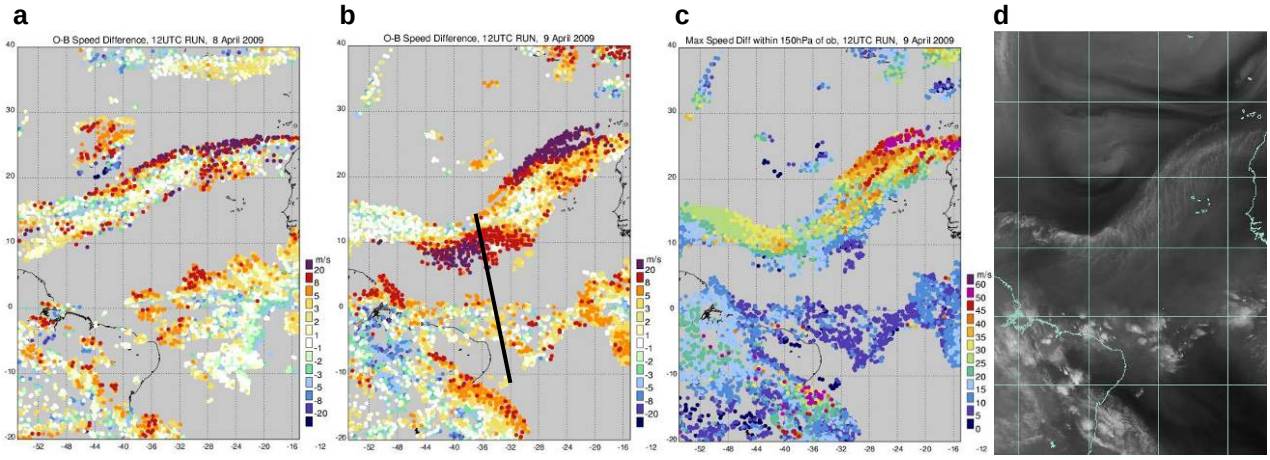

Figure 64: *O-B speed bias compared with the Met Office model background for (a) 1200 UTC on 8 April 2009 and (b) 1200 UTC on 9 April 2009 (black line marks the approximate location of the CALIPSO overpass in Figure 65). (c) Maximum speed difference within 150 hPa for Meteosat-9 WV 7.3 winds valid at 1200 UTC on 9 April 2009. (d) Meteosat-9 WV 6.2 image for 1200 UTC 9 April 2009, Copyright 2009 EUMETSAT/Met Office.*

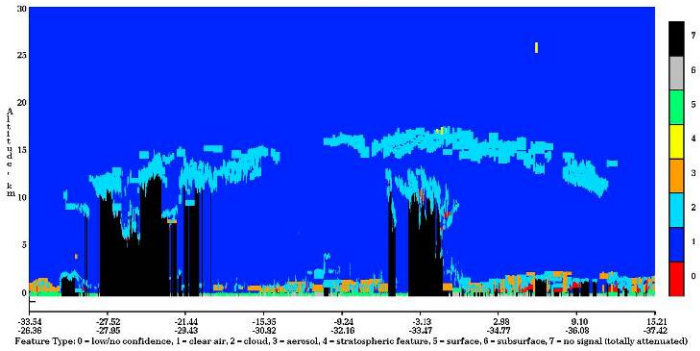

Figure 65: *CALIPSO cloud feature mask for approximately 1600 UTC 9 April 2009. Source: NASA. The clouds of interest are located on the right half of this image and the high level cloud corresponds roughly to the location of the black line drawn on Figure 64a.*

In summary, there are similarities in the relationship between these generally quite linear fast bias features and the clouds seen in the imagery. It is less clear what causes the bias, although in many instances it may be due to height assignment difficulties in cases of multi-layer or thin cloud. These result in bigger speed differences when strong vertical wind shear is present, possibly due to intrusion of energy into the tropics from mid latitudes.

4.2 GOES near equatorial slow bias

A slow speed bias is observed at high levels for edited and unedited GOES-11 and GOES-12 winds near the Pacific equator compared with the Met Office and ECMWF backgrounds (Figure 66). This feature is present in the IR and WV channels for January and February (and to a lesser extent March and April). The vector plots in Figure 67 show that the slow bias is associated with a region of moderate strength westerly winds located just north of the equator, with the flow diverging to become southwesterlies and northwesterlies to the north and south respectively. Divergence at high level is indicative of convergence below meaning this region is the likely position of the ITCZ.

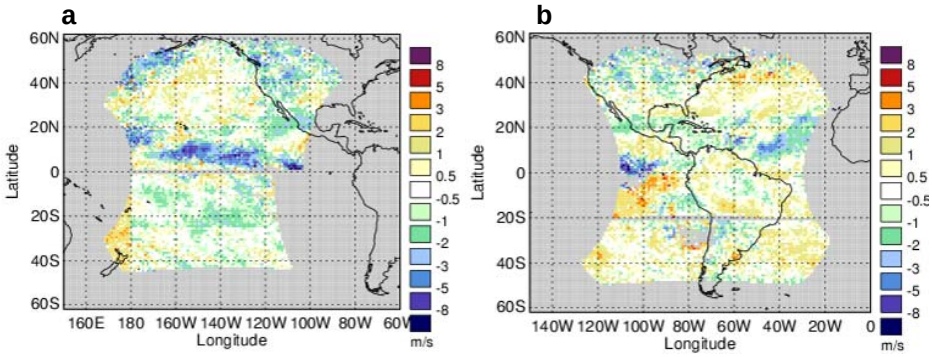

Figure 66: *Maps of O-B speed bias for (a) GOES-11 IR and (b) GOES-12 IR for January 2009 compared with the Met Office model background.*

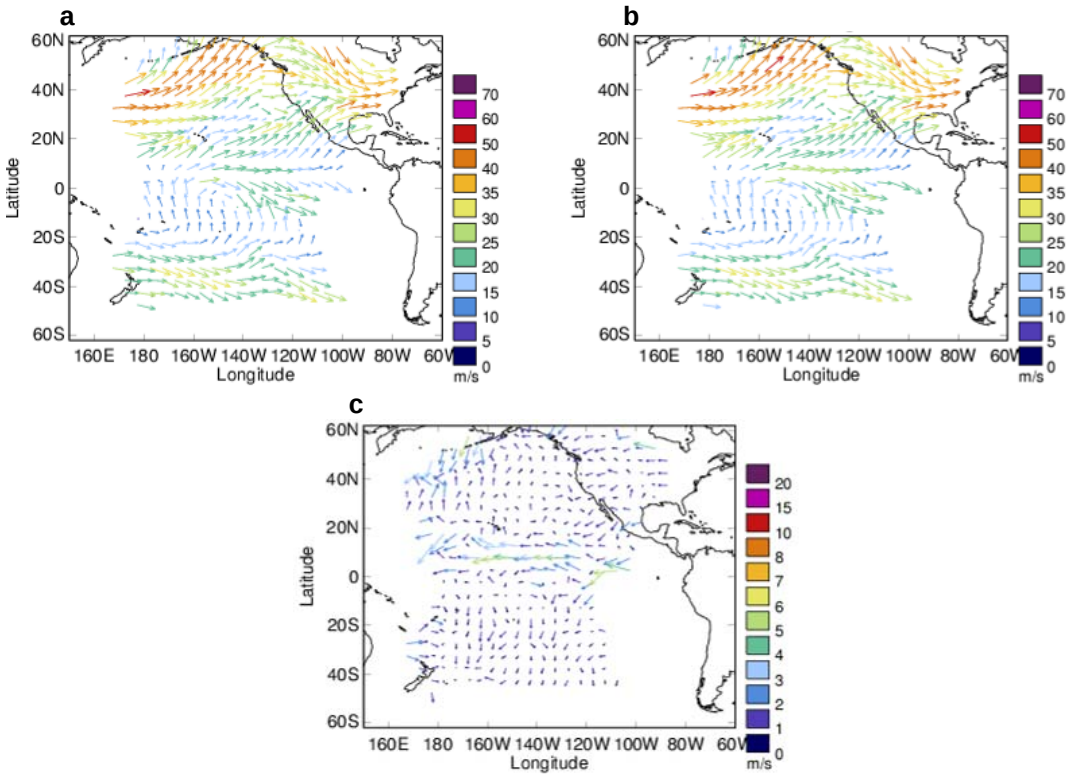

Figure 67: *Map plot of (a) mean observed vector, (b) mean Met Office model background vector and (c) mean vector difference for January 2009 for GOES-11 IR winds.*

Hovmöller plots of O-B speed bias show some day-to-day variation in the strength of the slow bias. A case at 00 UTC on 1 January 2009 was chosen for further investigation. Figure 68a shows the slow bias is located just north of the equator, to the southwest of Hawaii. IR satellite imagery for the same time and location (Figure 68b) shows a large area of convective activity associated with the ITCZ. A slow speed bias is located to the south and west, a fast bias is seen to the north and east. Looking at earlier images shows the slow bias increases as the system develops and grows over the preceding 12-24 hours. Interestingly the plots show a nearby group of AMVs tracking a separate streak of cloud (circled) moving west at around 3N which doesn't appear to be developing convectively and these instead show a neutral to slight fast bias.

It is not clear whether the bias relates to complications of tracking developing convective cloud, height assignment error, or possibly the model winds not capturing the flow correctly, although it is worth noting that both ECMWF and the Met Office show similar monthly O-B bias patterns in this region. Figure 67b shows the prevailing wind at this time of year is a moderate westerly near the equator which is stronger than at other times of the year. It is possible the bias relates to how this westerly flow is disturbed by a large, developing convective system. This fits with the observation that the nearby streak of cloud at 3N, which is not showing convective development, shows more neutral bias.

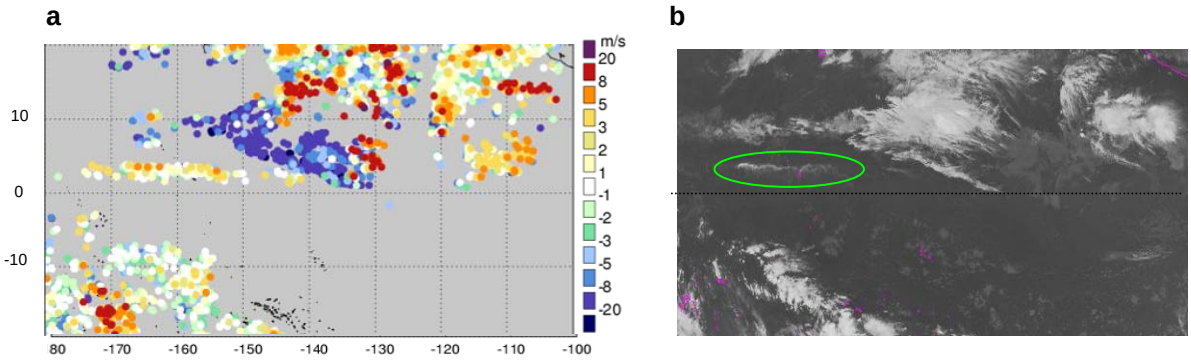

Figure 68: *(a) O-B speed bias compared with the Met Office model for high level unedited GOES-11 IR winds valid at 00 UTC on 1 January 2009. (b) GOES-11 IR imagery for the same area at 00 UTC.*

5.5. Polar winds

The NWP SAF monitoring covers a range of polar AMV datasets. These include data from CIMSS, direct broadcast stations and NESDIS MODIS with the latter split to show O-B monitoring for both the unedited and edited winds. Generally the statistics are similar for all datasets, but some differences are noted below.

Feature 4.3 Near-pole mid level slow bias

A small slow speed bias is seen at mid level polewards of ~80 N/S for some months; a feature which is slightly more prominent in the CIMSS-generated MODIS and AHVRR winds than the NESDIS MODIS winds (see Figure 69). Although not exclusively, the bias tends to occur more often during the winter months.

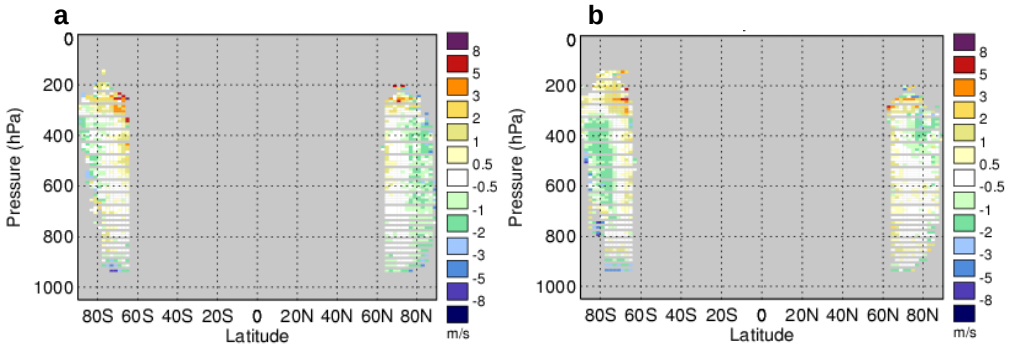

Figure 69: *Zonal O-B speed bias plots for (a) NOAA-18 IR winds for October 2008 and (b) CIMSS Aqua IR winds for August 2009, compared with the Met Office model background.*

The bias is not uniform for all longitudes (Figure 70). The example in Figure 70b shows an area of slow bias exceeding 5 m/s near zero degrees longitude in the SH.

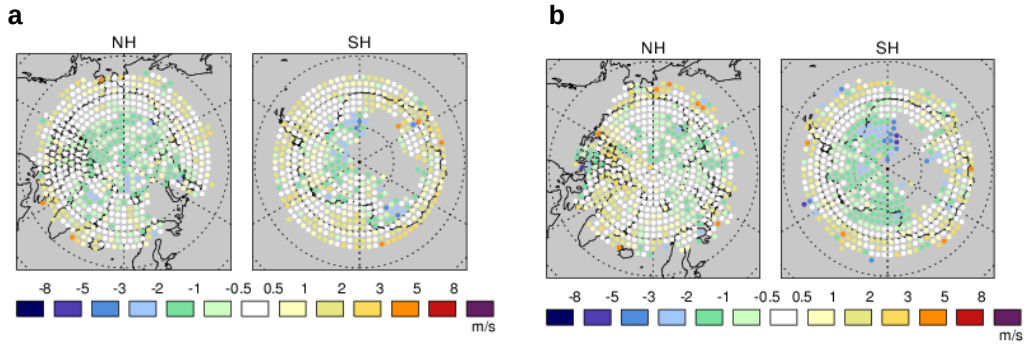

Figure 70: *Map O-B speed bias plots for (a) NOAA-18 IR winds for October 2008 and (b) CIMSS Aqua IR winds for August 2009, compared with the Met Office model background.*

Update on Feature 2.19. High level fast speed bias

A fast speed bias is seen at high levels in the edited polar IR and cloudy WV data, which is thought to be at least partly due to the speed increase in the autoeditor for winds faster than 10 m/s (see 3rd analysis report). Figure 71 shows an example for the AVHRR polar winds.

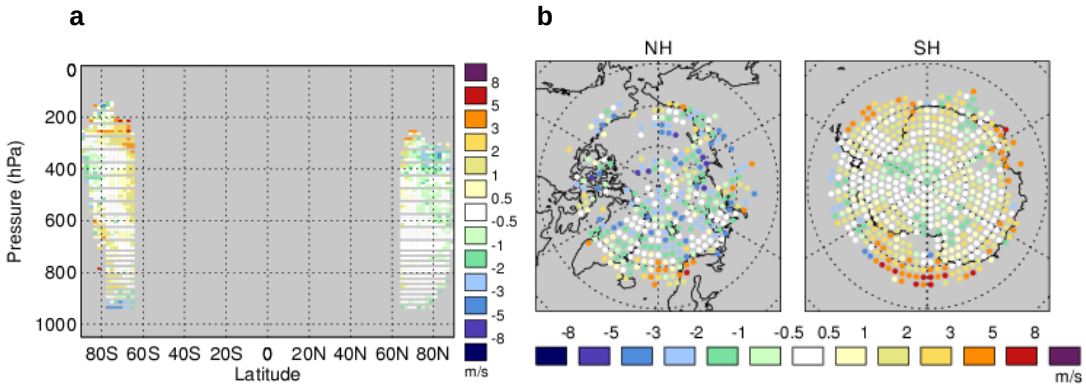

Figure 71: *(a) Zonal and (b) map O-B speed bias plots for NOAA-17 in September 2008 compared with the Met Office model background.*

The distribution of fast bias around the periphery of the SH polar disc can be investigated further by comparing the map plots of speed bias with mean 250 hPa Met Office analysis wind speed charts. Figure 72 shows examples for September and October 2008 for NOAA-17 IR winds.

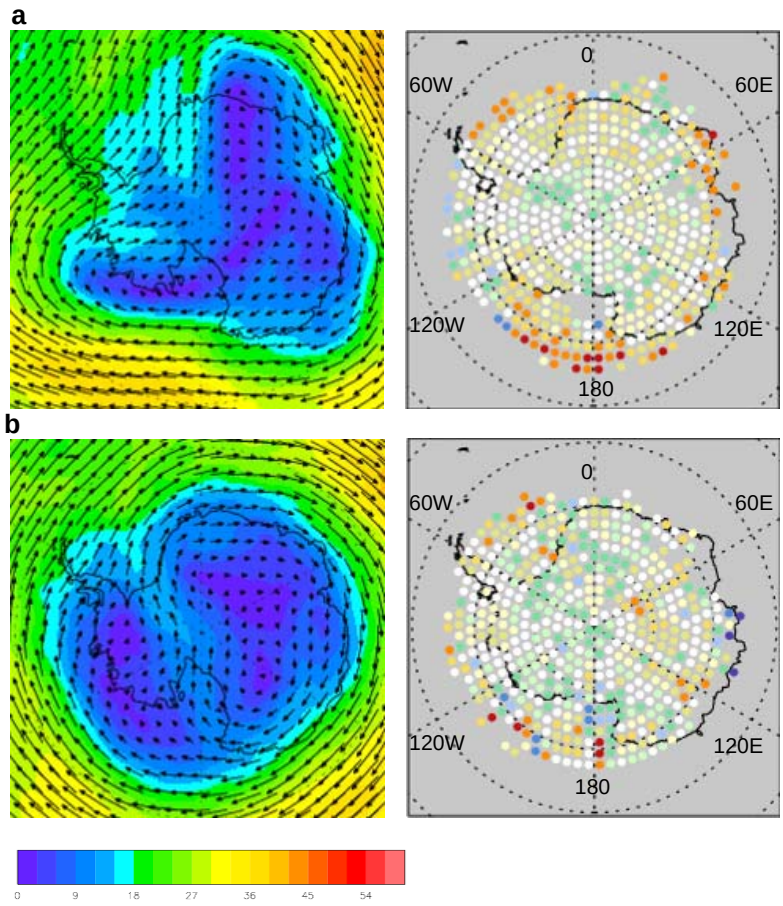

Figure 72 *Mean Met Office 250 hPa analysis wind speed (colour) and vector (arrows) for (a) September 2008 and (b) October 2008 together with the corresponding O-B speed bias plot for NOAA-17 IR winds in the same month.*

The O-B plot for September 2008 shows a bigger area of fast bias between 140W and 150E (going through 180) in comparison to October 2008. The mean analysis wind speed shows strong winds associated with the SH polar front jet circulating Antarctica but there is a difference in its location from month to month. Looking at the jet position near 180 degrees longitude shows that in September 2008 the faster winds have intruded much closer to the Antarctic continent in comparison to October 2008 and this may be responsible for the fast bias seen here.

Update on feature 2.20. Low level slow speed bias in polar IR data

A slow speed bias is seen below 900 hPa in both the edited and unedited polar IR datasets from NESDIS and CIMSS (e.g. Figure 73). The bias was exacerbated, until recently, in the NESDIS data due to a problem with very slow winds (Feature 3.4). Density plots for winds below 900 hPa (Figure 74) show the improvement in bias, particularly in the SH (-4.3 to -2.6 m/s) as a result of the removal of very slow winds in the NESDIS dataset. However, a more general slow bias remains. This bias tends to be worse at higher wind speeds and is also seen in equivalent plots for CIMSS-derived MODIS and AHVRR winds.

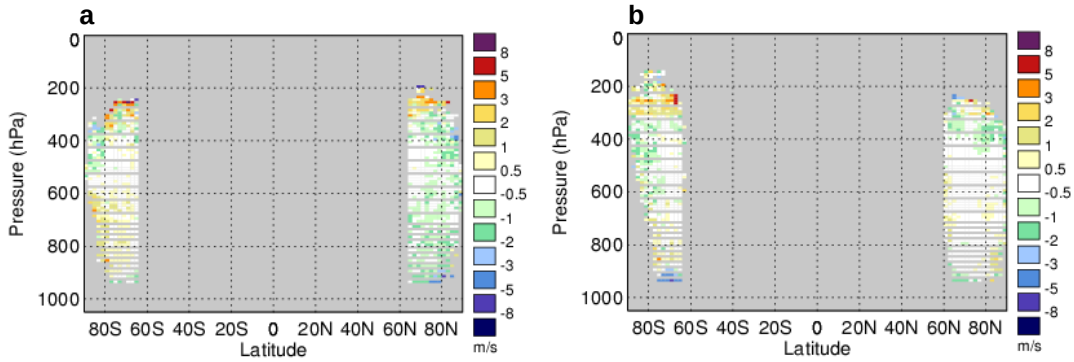

Figure 73: *Zonal O-B speed plots for NOAA-18 IR winds compared with the Met Office model for (a) January 2009 and (b) July 2009.*

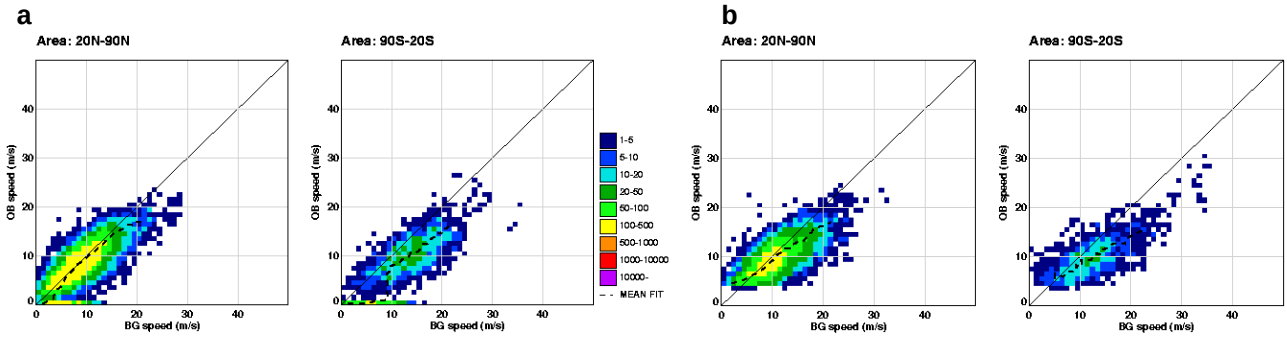

Figure 74: *Density plots of NESDIS Terra IR observation speed against Met Office model background speed for (a) October 2009 and (b) November 2009. The plots were produced after filtering to include only AMVs below 900 hPa.*

Update on feature 3.4. NESDIS MODIS IR slow streak

A streak of very slow AMVs was noted in the 3rd analysis report at all levels for the NESDIS MODIS IR data. This can be seen in the density plots for October 2009 in Figure 75a. On the 27 October 2009 NOAA/NESDIS implemented a change to the MODIS polar winds processing to remove winds with speeds of less than 4 m/s. Figure 75b for the beginning of November 2009 shows that this fix has had the desired effect with all the slowest winds removed from the data.

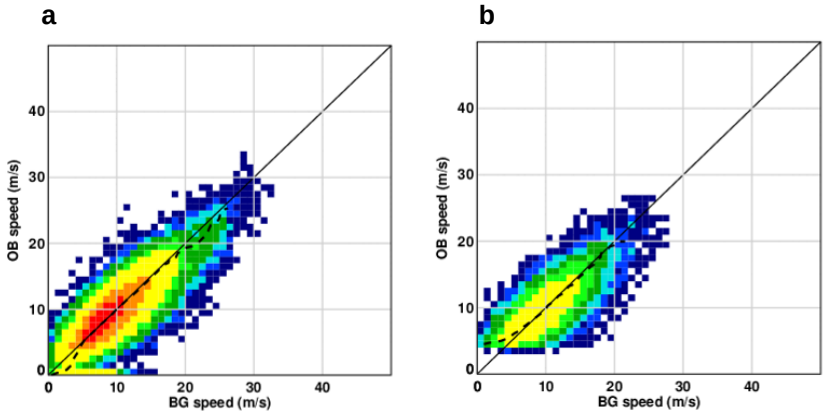

Figure 75: *Speed bias density plots for NESDIS Aqua IR NH low level winds for (a) October 2009 and (b) November 2009 compared with the Met Office model background.*

The reason why these slow winds are generated is probably due to tracking of stationary surface features, which may show small movement between images due to navigation error. The slow winds are nearly all less than 1 m/s. The exception is for NOAA-18 in March 2009 when a slow bias streak (observation speeds of 4-5 m/s and model background speeds of up to 23 m/s) was seen in the NH despite speed thresholding of 4 m/s being applied at CIMSS (Figure 76). On further investigation this signal comes entirely from one batch of data valid at 2135-2140 on 24 March 2009 and may relate to larger navigation errors on this occasion.

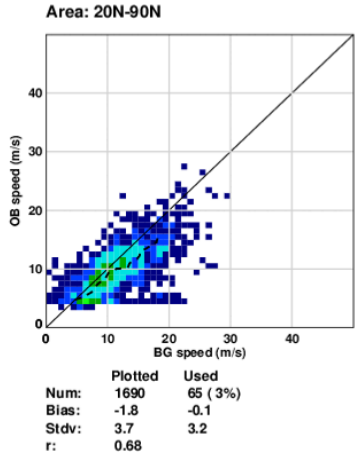

Figure 76: *Density plot of NOAA-18 AMV observation speed against Met Office model background speed for March 2009 in the NH. The plot was produced after filtering to include only AMVs below 900 hPa.*

6. Conclusions

The NWP SAF AMV monitoring site has improved in several ways since the 3rd analysis report of February 2008. These are described in Section 2 and include an upgrade to the site navigation, the addition of follow-up investigations on specific aspects of the AMV monitoring and updates to the information on how AMVs are used in different global NWP systems.

The AMV analysis report continues to deliver feedback on new observation types (Section 4) providing guidance for NWP centres considering assimilating new AMV datasets as well as feedback to the data producers. AMVs from NOAA-19 and the new direct broadcast MODIS/AVHRR winds should improve polar AMV coverage and resilience in NWP models. Rapid scan winds such as those from Meteosat-8 have the potential to provide information on the local wind field but more work is required to refine their derivation and also to adapt the NWP assimilation and quality control to optimise impact in high resolution NWP.

A key focus of the NWP SAF AMV analysis reports is the maintenance of a record of features identified in the O-B monitoring (Section 5). The plots versus the Met Office and ECMWF models are usually very similar suggesting that AMV errors dominate in most cases. Model errors make a smaller contribution but are still present as shown by Feature 4.1. The O-B speed biases can often be explained by systematic height assignment errors. In some cases investigations have highlighted possible causes and solutions. For example, the mid level slow bias in the extratropics for Meteosat-9 is worse for AMVs assigned a height using the CO_2 slicing method (Feature 2.9). Currently the choice of height assignment method is controlled by a temperature threshold alone, however model best-fit pressure investigations suggest substantial improvements to the statistics if a CO_2 pressure threshold is applied as well. This is probably also applicable to GOES AMVs.

Improvements to AMV derivation often have a visible impact on the O-B statistics. Features such as the MTSAT-1R mid level fast bias (3.1) and the NESDIS MODIS IR slow streak (3.4) have either been removed or considerably reduced. However, many of the bias features described in earlier analysis reports persist. The most prevalent problems remain the fast bias in the tropics (Features 2.8 and 2.13) and the slow bias in the jet regions (Features 2.9 and 2.10) at both mid and high levels. They often relate to difficulties in height assignment in multi-level cloud regions and the bias is often exacerbated by high vertical wind shear. Improvements should be seen from more accurate height assignments and by identifying less-trusted observations so that they can be downweighted (through more realistic representation of the observation errors) or blacklisted in NWP.

The NWP SAF AMV analysis reports, monthly monitoring pages and investigations aim to improve knowledge of the AMV errors and help focus areas of development in the AMV derivation and assimilation. It is hoped that these resources will stimulate discussion and further investigation within the AMV community.

Appendix 1: Revised Action List

The NWP SAF AMV action list can be viewed at: http://www.metoffice.gov.uk/research/interproj/nwpsaf/satwind_report/action_list.html; the completed actions are available as a link from this page. The action list is updated every few months and is fully revised on the completion of each analysis of results. The revised action list is included below and provides suggestions of possible developments to the site and ideas for investigating some of the observation-background inconsistencies further. It is important to realise that the items in the action list represent ideas for future work as opposed to a formal task list. The items will be addressed, when time allows, in priority order. We welcome feedback including any additional suggestions for follow-up work.

A1.1. Discrepancies between contributors

Ref	Action	Details	Centre(s)
1.9	ECMWF to provide polar map data using distance bins	A one degree grid is used for the geostationary data, but this is less meaningful over the poles. Instead the Met Office polar map plots use a distance box.	ECMWF

A1.2. Improvements to site design

Ref	Action	Details	Centre(s)
2.10	Expand analysis web page	Provide reference to what is included in each analysis report.	MetO
2.11	Add real-time monitoring	Currently provide links to other sites - could add some basic plots for the Met Office (ECMWF covered elsewhere).	MetO
2.12	Display examples of plot output	The AMV monitoring/analysis system has been developed over a number of years to help with the biennial analysis and other investigations. We could add a new tab to highlight the range of plots that can be produced.	MetO
2.13	Summaries of AMV	e.g. quality problems in day-to-day monitoring	MetO

	events	and monitoring changes following derivation updates. Probably include as a section under investigations.	

A1.3. Development of plots

Ref	Action	Details	Centre(s)
3.10	Develop time series and/or Hovmöller plots	These can be produced at the Met Office (by latitude or pressure) and can be useful for investigating day-to-day variability in O-B stats. They have not been added yet due to the large number of plots already displayed.	MetO, ECMWF
3.11	Develop plots comparing AMVs to other observations	Lower priority unless strong demand	MetO, ECMWF
3.12	Inclusion of plots from other centres	Guidance available. Awaiting provision of data from other NWP centres. Lower priority due to similarity of Met Office and ECMWF plots.	MetO and other contributors

A1.4. Analysis of results

Ref	Action	Details	Centre(s)
4.2	Provide routine updates	Update analysis every two years. Update action list every 6 months or when significant changes take place.	MetO

A1.5. Follow up investigations

Ref	Action	Details	Centre(s)
5.7	General height assignment investigations	Continue investigations into differences between channels and satellites in regions of overlap and comparisons with model best-fit pressure.	MetO, ECMWF

Acknowledgements

We would like to thank Antonio Garcia-Mendez for providing the ECMWF monthly statistics, Robert Tubbs for managing the NWP SAF website and Roger Saunders and John Eyre for suggestions to improve this document. The work has also benefited from discussions with data providers, in particular EUMETSAT and CIMSS.

References

Bedka, K.M., and J.R. Mecikalski, 2005. Application of Satellite-Derived Atmospheric Motion Vectors for Estimating Mesoscale Flows. *J. Appl. Meteor., **44**, 1761–1772.*

Borde R., and R. Oyama, 2008. A Direct Link between Feature Tracking and Height Assignment of Operational Atmospheric Motion Vectors. *Ninth Int. Winds Workshop, Annapolis, USA.*

Bormann, N., C. Delsol and J-N Thépaut, 2006. Challenges and plans for the assimilation of atmospheric motion vectors at ECMWF. *Proceedings of the 8th International Winds Workshop, Beijing, available from EUMETSAT, Darmstadt, Germany.*

Forsythe, M. and M. Doutriaux-Boucher, 2005. Second analysis of the data displayed on the NWP SAF AMV monitoring website. *NWP SAF Technical Report 20, available at http://www.metoffice.gov.uk/research/interproj/nwpsaf/satwind_report/nwpsaf_mo_tr_020.pdf.*

Forsythe, M. and R. Saunders, 2008. Third analysis of the data displayed on the NWP SAF AMV monitoring website. *NWP SAF Technical Report 22, available at http://www.metoffice.gov.uk/research/interproj/nwpsaf/satwind_report/nwpsaf_mo_tr_022.pdf.*

Galante Negri, R. and M. Forsythe, 2009. Synoptic assessment of AMV errors. *NWP SAF visiting scientist report, available at http://www.metoffice.gov.uk/research/interproj/nwpsaf/vs_reports/nwpsaf-mo-vs-038.pdf*

Griersmith, D., 2008. Status report on the Global RARS initiative. *Proceedings of the 16th International TOVS Study Conference, Angra dos Reis, Brazil.*

Hewison, T. and M. König, 2008. Inter-calibration of Meteosat imagers and IASI. *Proceedings of the EUMETSAT Satellite Conference, Darmstadt, Germany, September 2008*.

Holmund, K., 1998. The utilisation of statistical properties of satellite-derived atmospheric motion vectors to derive quality indicators. *Weather Forecasting*, **13**, 1093-1104.

Holmlund, K. and J. Schmetz, 1990. Cloud displacement as a representative of the wind field. *Proceedings of the 8th Meteosat Scientific Uses Meeting, Sweden, available from EUMETSAT, Darmstadt, Germany.*

Key, J., W. Straka III, D. Santek, C. Velden and R. Dworak, 2006. Satellite-derived winds at direct broadcast sites in the polar regions. *Proceedings of the 8th International Winds Workshop, Beijing, available from EUMETSAT, Darmstadt, Germany.*